PREDICTING FATIGUE LIFE OF A MOUNT OF A DEVICE WITH SHOCK ABSORBER

ŞOK SÖNÜMLEYİCİYE SAHİP CİHAZIN MONTAJ ARAYÜZÜNÜN YORULMA ÖMRÜNÜN HESAPLANMASI

UĞUR TEKECİ

PROF. DR BORA YILDIRIM

Supervisor

Submitted to

Graduate School of Science and Engineering of Hacettepe University

As a Partial Fulfillment to the Requirements for the Award of the Degree of Master of Science in Mechanical Engineering.

2022

ABSTRACT

PREDICTING FATIGUE LIFE OF A MOUNT OF A DEVICE WITH SHOCK ABSORBER

Uğur TEKECİ

Master of Science Degree, Department of Mechanical Engineering

Supervisor: Prof. Dr. Bora YILDIRIM

August 2022, 46 pages

All aircraft operate under vibration loads and these loads cause vibration-induced fatigue damage to the parts. Fatigue damages are dangerous because they occur suddenly without giving a warning before, for this reason they need to be carefully analyzed. In the analysis, especially the natural frequencies and dampings must be determined correctly, because when the vibration loads match with the natural frequencies, resonance is observed and this reduces the life of the part.

In this thesis, the fatigue life of a mount of device with shock absorber is investigated. Flight tests were carried out in real flight scenarios to provide an input for the analysis.

A modal test was performed to model the shock absorbers correctly. Vibration test was performed to prove the accuracy of the prepared finite element model and to determine the damping ratios.

Fatigue analyses were performed in frequency domain with a commercial software, nCode, and the accuracy of the analysis was proven by the test.

Keywords: Fatigue Analysis, Shock Absorber, Finite Element Method

ÖZET

ŞOK SÖNÜMLEYİCİYE SAHİP CİHAZIN MONTAJ ARAYÜZÜNÜN YORULMA ÖMRÜNÜN HESAPLANMASI

Uğur TEKECİ

Yüksek Lisans, Makine Mühendisliği Bölümü

Tez Danışmanı: Prof. Dr. Bora YILDIRIM

Ağustos 2022, 46 sayfa

Hava araçları titreşim yükleri altında çalışmaktadır ve bu yükler parçalarda titreşim kaynaklı yorulma hasarına sebep olmaktadır. Yorulma hasarları öncesinde bir uyarı vermeden aniden oluşması nedeniyle tehlikeli hasarlardır bu yüzden dikkatlice analiz edilmesi gerekmektedir. Analizlerde özellikle doğal frekansların ve sönümlemelerin doğru belirlenmesi gerekir çünkü titreşim yüklerinin doğal frekanslarla çakışması durumunda rezonans gözlenir ve bu parçanın ömrünü azaltır.

Bu tez kapsamında şok sönümleyiciye sahip bir cihazın montaj arayüzünün yorulma ömrü analiz edilmiştir. Analize girdi olması amacıyla gerçek uçuş senaryolarında uçuş testleri gerçekleştirilmiştir.

Şok sönümleyicilerinin doğru modellenmesi için modal test yapılmıştır. Hazırlanan sonlu elemanlar modelinin doğruluğunu kanıtlamak ve sönümleme oranlarının tespiti için titreşim testi yapılmıştır.

Yorulma analizleri ticari bir yazılım olan nCode ile frekans düzleminde yapılmış ve analizin doğruluğu yapılan test ile kanıtlanmıştır.

Anahtar Kelimeler: Yorulma Analizi, Şok Sönümleyici, Sonlu Elemanlar Modeli

ACKNOWLEDGEMENTS

I would like to express my gratitude to my thesis supervisor Prof. Dr. Bora Yıldırım for his guidance, support, contributions and trust in me throughout this thesis.

I want to thank my colleagues Ahmet Özdemir and Öner Murat Akbaba for their helpful advice and support.

I want to thank my managers and ASELSAN Inc. for giving me the opportunity to use the testing laboratories during my thesis.

I would like to express my eternal appreciation towards my dear mother, father and sisters, who helped me to come to these days and always put trust in me.

Finally, huge thanks to my beloved wife Cansel Şahin Tekeci for her endless love, unconditional moral support and patience during the thesis.

Table of Contents

1. INTRODUCTION 1
1.1. Fatigue Phenomena 1
1.2. History of Fatigue Research 2
1.3. Thesis Outline 3
2. LITERATURE SURVEY 4
2.1. Fatigue 4
2.2. Isolator Modeling 5
3. FATIGUE THEORY 8
3.1. Damage Theories 8
3.1.1. Stress Life Approach 8
3.1.2. Strain Life Approach 17
3.1.3. Crack Propagation Approach 18
3.2. Random Vibration Fatigue 18
4. FLIGHT DATA ACQUSITION 20
5. VIBRATION FATIGUE ANALYSIS AND VERIFICATION 23
5.1. Finite Element Model Preparation 23
5.2. Absorber Model 25
5.3. Finite Element Model 28
5.4. Fatigue Life Analysis 31
5.5. Accelerated Life Test 36
5.6. Case Study I 37
5.7. Case Study II 38
6. CONCLUSION AND DISCUSSION 39
REFERENCES 41
APPENDICES 44

LIST OF FIGURES

Figure 1.1 Unnotched 2024-T4 Aluminum Alloy S/N Curve 1
Figure 2.1 Typical Vibration Isolation Systems 5
Figure 2.2 Single Degree of Freedom Voigt Model 7
Figure 3.1 Fatigue stress cycles 8
Figure 3.2 S/N curves for ferrous and non ferrous metals 9
Figure 3.3 Soderberg, Goodman and Gerber approaches [33] 10
Figure 3.4 Stress cycles encountered by an airplane for different flight regimes [34] 11
Figure 3.5 Rainflow cycle counting method [36] 13
Figure 3.6 Range-Mean Histogram of rainflow cycle counted data [37] 14
Figure 3.7 Principal Stress vs biaxiality ratio and principal stress angle for multiaxial proportional loadings [38] 15
Figure 3.8 Principal Stress vs biaxiality ratio and principal stress angle for multiaxial non-proportional loadings [38] 16
Figure 3.9 Equivalent stress theories for a cylindrical notched specimen with uniaxial sine loading [39] 17
Figure 4.1 Acceleration PSD's 21
Figure 4.2 PSD Envelope 22
Figure 4.3 PSD Comparison for 2500 and 4 Hours 23
Figure 5.1 CAD Model of Test Setup 23
Figure 5.2 Simplified ANSYS Model 24
Figure 5.3 Meshed Model 25
Figure 5.4 Test for Obtaining the Absorber Characteristics 25
Figure 5.5 PSD Comparison for Model and Test Results in X-Direction 26
Figure 5.6 PSD Comparison for Model and Test Results in Y-Direction 27
Figure 5.7 PSD Comparison for Model and Test Results in Z-Direction 27
Figure 5.8 Responses for Different Input Loadings 28
Figure 5.9 White Noise Vibration Test 29
Figure 5.10 Mode Shapes of Structures 29
Figure 5.11 Sensor 1 Test vs ANSYS Comparison 30
Figure 5.12 Sensor 2 Test vs ANSYS Comparison 30
Figure 5.13 ANSYS Workbench – Ncode analysis construction 31
Figure 5.14 Lalanne Method Fatigue Life Result 32

Figure 5.15 Dirlik Method Fatigue Life Result 33
Figure 5.16 Narrow Band Method Fatigue Life Result 33
Figure 5.17 Stress PSD for 2500 Hours Input PSD 34
Figure 5.18 RMS Stesses for 2500 Hours Input PSD 34
Figure 5.19 Dirlik Method Damage Histogram 35
Figure 5.20 Dirlik Method Damage Histogram 35
Figure 5.21 Fracture on the Mount and Finite Element Model 37
Figure 5.22 ANSYS Model of the System Without Absorbers 37

LIST OF TABLES

Table 3-1 The output of a rainflow cycle counted data [36] 13
Table 3-2 Combination methods according to proportionality [23] 16
Table 4-1 Flight Conditions and Durations 20
Table 5-1 Experiment Amplitudes and Corresponding Damping Ratios 28
Table 5-2 Comparison of Natural Frequencies and Damping Ratios 31
Table 5-3 Fatigue Life Analysis Results for 2500 Hours PSD 32
Table 5-4 Fatigue Life Analysis Results for 4 Hours PSD 36
Table 5-5 Fatigue Life Analysis Results for Test PSD 36
Table 5-6 Fatigue Life Analysis Results for the Mount Without Absorbers 38
Table 5-7 Fatigue Life Analysis Results for Diffrent m Values 38
Table B-1 Material Properties of Aluminum 2024 T3 45
Table B-2 Material Properties of Aluminum 6061-T6 46

LIST OF SYMBOLS & ABBREVIATIONS

List of Symbols

σ_{min}	Minimum Stress
σ_{max}	Maximum Stress
σ_r	Stress Range
σ_m	Mean Stress
σ_a	Alternating Stress
R	Stress Ratio
A	Amplitude Ratio
N	Number of Cycle According to S-N Curve
C	Material Constant
b	Basquin Exponent
S_e	Modified Endurance Limit
S'_e	Endurance Limit
k_a,k_b,k_c,k_d,k_e,k_f	Endurance Limit Modification Factors
K_t, K_{ts}	Stress Concentration Factors of Normal and Shear Stresses
K_f, K_{fs}	Fatigue Stress Concentration Factors of Normal and Shear Stresses
q	Notch Sensitivity
σ_{UTS}	Ultimate Tensile Strength
σ_Y	Yield Strength
σ_0	Fatigue Strength
$[ED]$	Total Accumulated Damage
σ_1, σ_2, σ_3	Maximum, Intermediate and Minimum Principal Stress
σ_{xx}, σ_{yy}, σ_{zz}	Normal Stresses in x, y and z direction
σ_{xy},σ_{xz},σ_{yz}	Shear Stresses
a_e	Biaxiality Ratio
ϕ_p	Principal Stress Angle
σ_{AMP}	Absolute Maximum Principal Stress
σ_{SVM}	Signed Von Mises Stress
σ_ϕ	Critical Plane Stress
$y(f_n)$	Frequency Domain Transferred Signal
$y(t_k)$	Time Domain Transferred Signal

m_n	Spectral Moments of Stress PSD
Δf	Frequency Increment
$G(f)$	Response PSD function
$E[0]$	Expected Number of Zero Crossings per Second
$E[P]$	Expected Number of Peaks per Second
γ	Irregularity Factor
x_m	Mean Frequency of PSD Response
S	Stress
$p(S)$	Probability Density Function
$n(S)$	Number of Cycle
T	Random Load Exposure Duration
$D(f_n)$	Fatigue Damage Spectrum
k	Constant of Proportionality
ζ	Damping Ratio
Γ	Gamma Function
$DP(f_n)$	Damage Potential Spectrum
m	Accelerated Life Testing Formula Exponent

List of Abbreviations

PSD	Power Spectral Density
FFT	Fast Fourier Transform
FRF	Frequency Response Function
TF	Transfer Function
RMS	Root Mean Square
FDS	Fatigue Damage Spectrum
FEA	Finite Element Analysis
CAD	Computer Aided Design
gRMS	Root Mean Square Acceleration

1. INTRODUCTION

1.1. Fatigue Phenomena

Most of the machine elements consist of metallic parts and these parts generally work under cyclic or fluctuating loads. Although these loads do not cause the parts to break immediately, they can cause damage to the part after a certain amount of cycles. This is called the fatigue phenomenon in the literature.

Fatigue failures are dangerous as even relatively low loads can cause a sudden failure without warning. Fatigue analysis is important to ensure that the machines will complete their specified service time without failure.

In order to determine the fatigue strength of materials, testing under different conditions is required. The life of the materials varies according to the stress ratio and amplitude. The figure below shows the S/N graph of 2024AL taken from MIL-HDBK-5J.

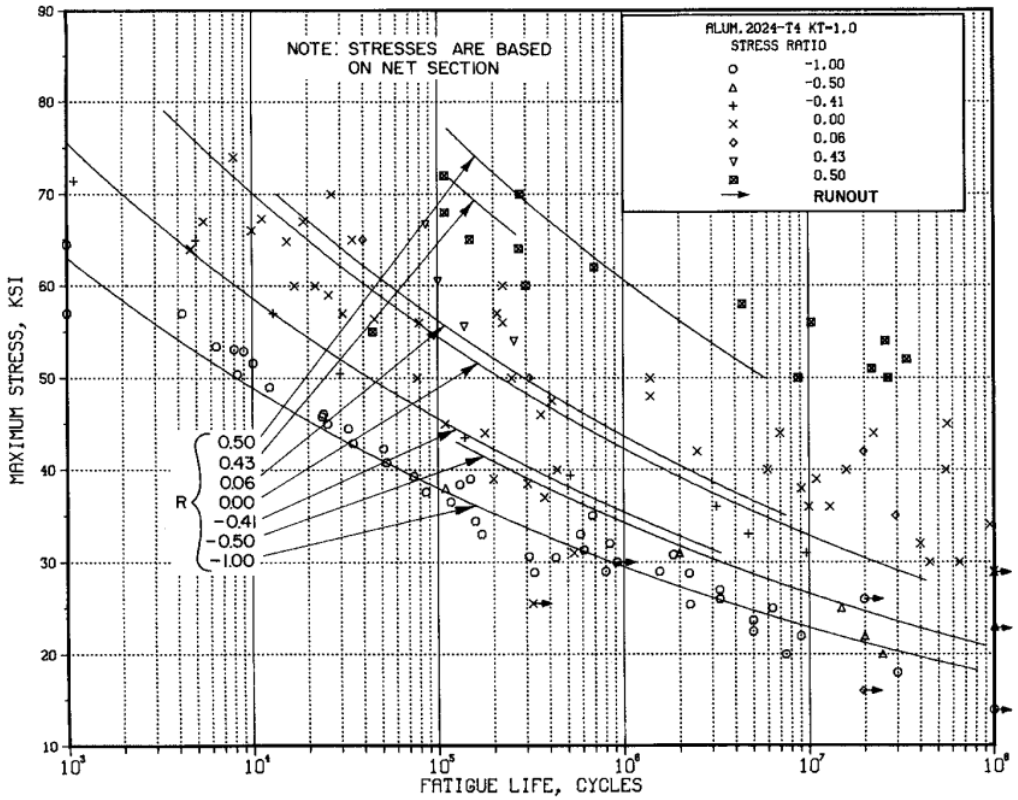

Figure 1.1 Unnotched 2024-T4 Aluminum Alloy S/N Curve [45]

1.2. History of Fatigue Research

Studies that investigate the cause of failure of materials, that happen under loadings not even exceeding the yield strength, began in the 1800s.

- The first person to mention the fatigue phenomenon is the German engineer Wilhelm Albert, who investigated the failure of crane chains in mines [1].
- In a lecture at the military school in Metz, Jean-Victor Poncelet described metals as "tired" materials [2].
- The fatigue strength of railway axles and importance of stress concentration was discussed in 1842 by Scottish William John Macquorn Rankine [3].
- In1860, Sir William Fairbairn and August Wohler conducted the first systematic fatigue life studies. Wöhler's work on railway axles leads him to the idea of the fatigue limit and to propose the use of S-N curves in mechanical design [4].
- In 1899, work on the relationship of fatigue life to mean and alternating stresses was published by Goodman [5].
- Ewing shows that fatigue failure is caused by microscopic cracks, in 1903 [6].
- In 1910, O. H. Basquin constructed the form of a typical S-N curve [7].
- In 1924, Englishman Gough published the first fatigue book [8].
- An article published on damage accumulation hypotheses for fatigue life by Palmgren in 1924 [9].
- The linear damage hypothesis was first published by A.Palmgren in 1924 and was further popularized by M.Miner in 1945 [10].
- In 1954, L. F. Coffin and S. S. Manson's performed studies on the relationship between plastic strain and fatigue life in the low-cycle high-strain fatigue regime. [11] [12].
- Studies on the growth of cracks due to variations in loads were published by Paris in 1962 [13].
- The Rainflow-Counting algorithm was developed by Tatsuo Endo and M. Matsuishi in 1968. It became the first accepted method to extract closed loading reversals or cycles. [14].
- The phenomenon of crack closure was first discovered by Elber in 1970 [15].

1.3. Thesis Outline

This thesis consists of six chapters. In the first chapter, information about the fatigue phenomenon is given briefly and the dangers of fatigue are mentioned. Some important studies on metal fatigue are written in chronological order.

In the second chapter, the literature research was done on two different topics. Firstly, important studies on vibration-based fatigue and studies related to fatigue analysis covered in this thesis are given. Afterwards, studies on isolator modeling were investigated.

The next section provides more information on details of metal fatigue. Three different approaches of damage theory are covered separately. Stress life theory is explained in detail; others are briefly mentioned. Finally random vibration fatigue is explained in detail.

In the fourth chapter, how to create the PSD graph of the flight profile is explained. Test results in different directions are given in graphs. Amplifying the existing PSD to be used in fatigue tests is described.

The fifth chapter consists the analyzes and tests performed within the scope of this thesis and the results of them. The mesh and connections used in the construction of the FEM are mentioned. The details of modeling the absorbers and calculating the damping ratios are given. To show the accuracy of the finite element model, a comparison was made with the test results. Fatigue analysis is performed with three different methods and comparative results are given. The analysis results are verified with the accelerated life test. Finally,two study cases are given

In the last section, the studies for the thesis are mentioned and the results are interpreted.

2. LITERATURE SURVEY

2.1. Fatigue

Rice published a correlation between spectral moments of stres PSD and upward mean crossings peaks [16].

In 1964, Bendat [17] presented the Probability Density Function of rainflow intervals in the frequency domain for narrowband signals using the first four spectral moments of the stress power spectral density function. This method, which gives good results for narrow bands, is very conservative for wide bands.

Many methods have been developed to correct this conservatism. Tunna [18], Wirsching [19] and Chaudhury & Dover [20] have presented methods in order to improve Bendat's narrowband method. Also, Steinberg proposed three-band technique whih is a simplified fatigue life prediction procedure for electronic components [21].

Dirlik [22] proposed an empirical closed form expression using Monte Carlo technique and computer simulations. This expression gives the probability density function of rainflow ranges. In wideband and narrowband signals, Dirlik's method gives accurate results and used in many fatigue life studies.

Bishop [23] performed some studies frequency and time domain based fatigue techniques in finite element environment. It is stated that, to add the dynamics of the structure to the time domain, a transient dynamic analysis must be performed, which requires a very long time and is sometimes practically impossible to implement. Spectral methods using the random vibration theory can be used, instead of the time domain methods.

Aykan [24] analyzed a bracket which is belong to a helicopter's self-defense system's chaff/flare dispenser by using vibration fatigue method. From operational flight tests, acceleration power spectral density is obtained. Finite element model of the bracket is constructed to get stress power spectral density. The finite element model has been verified by the results obtained from the experiments.

Eldogan [25] developed a numerical code that is capable of analyzing the fatigue life of structures both in frequency domain and time domain. Flight data is acquired from the aircraft and analyzes are performed with this data. For time domain analysis, stress history is obtained using strain gauges placed at the critical locations of the part. On the other hand, in the frequency domain analysis, stress PSDs are obtained in finite element model of structure

hereby before obtaining stress PSDs, finite element model is verified with experiments. Fatigue life which is found from the developed code and commercial software is compared with experimental fatigue life tests in order to verify the results. When comparing the frequency domain and time domain results, Dirlik's method gives the best results with the rainflow cycle counted time domain analysis.

2.2. Isolator Modeling

Kelly [26] and Silva [27], basically have grouped the vibration isolation problems into two branches:

- Protection of foundation against large forces of equipment (Figure 2-1a);
- Protection of equipment against motion of foundation (Figure 2-1b).

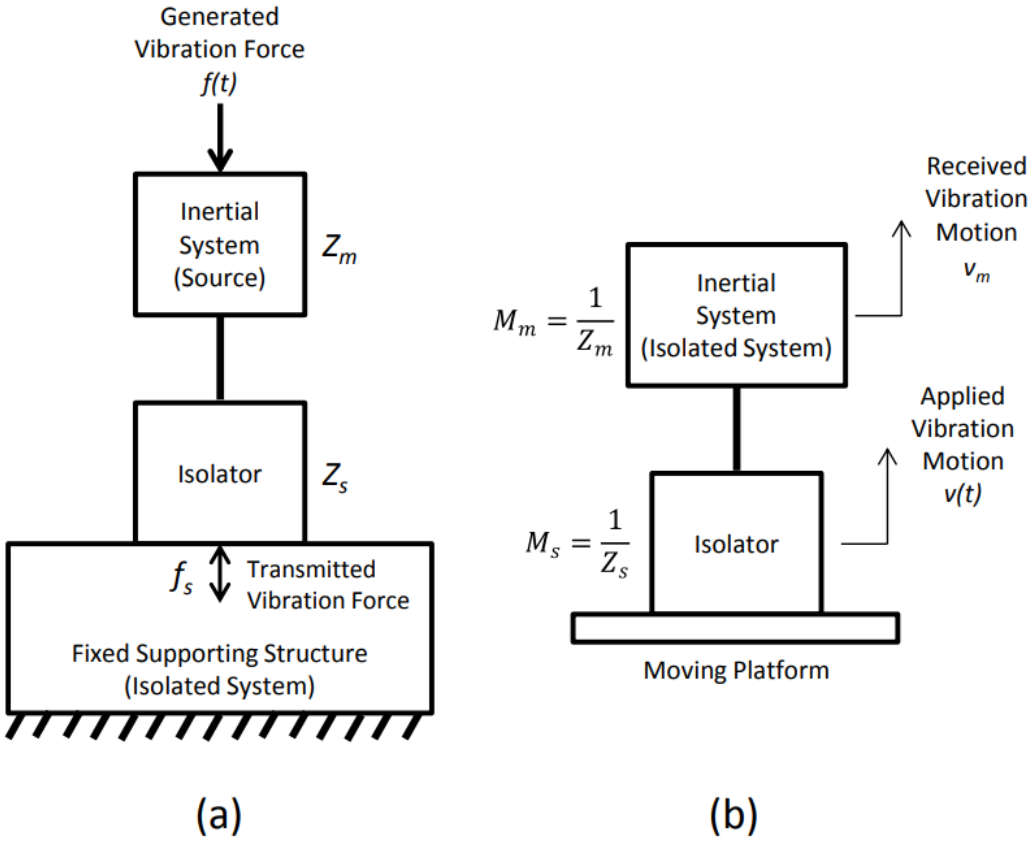

Figure 2.1 Typical Vibration Isolation Systems [27]

For these problems, Kelly [26] and Rao [28] presented the vibration control methods below.

- Elimination of the external vibration input or reduction in its amplitude,
- Adjusting system characteristics such as inertia, stiffness and damping by an optimized structural design,
- Reduction of force or motion transfusion by the use of absorbers or vibration isolators mounted on the mechanical structure.

The first process is based on the vibration source. The amplitude of vibration source should be reduced directly or the location of the device should be changed away from the sources of excitation. Because of the assembling necessity for the device and not preferred direct intervention to the vibration source, the method is considered as improper.

The second method is based on the structural reinforcement. This method can be used effectively in the design phase. However, it cannot be used on a device whose design and production have been completed.

The third method is the most preferred method on this type of devices. In this process, diminution in the dynamic response of the structure is obtained by using a variety of components like springs, resilient members, auxiliary mass damper, pneumatic or hydraulic mounts. Also, as Rao [28] mentions, the isolation system is decribed as passive or active depending on the necessity of external control of the devices to perform their functions.

In passive vibration isolation systems, a resistant force across the device without any use of power supply produced by isolators. There are different types of passive vibration isolators in the literature. Nevertheless, for all types, an energy dissipater or a force resistance element is common. Pneumatic springs, metal springs, elastomer springs in addition to wire rope isolators, elastomeric pads and sheets and negative-stiffness isolators can be given as examples used in passive vibration isolation systems.

The Voigt model is frequently used for elastomeric isolator modeling due to its simplicity in parameter and analysis identification. [29]. The Voigt model is a two-element model with a spring and a viscous damper as shown below. Since the elastomer is a viscoelastic polymer, the Voigt model can be used in a limited area. On the other hand, Zhang and Richards [30] proposed that, dynamic stiffness experiments show the frequency dependent features of elastomeric isolators and thus the Voigt model is not sufficient.

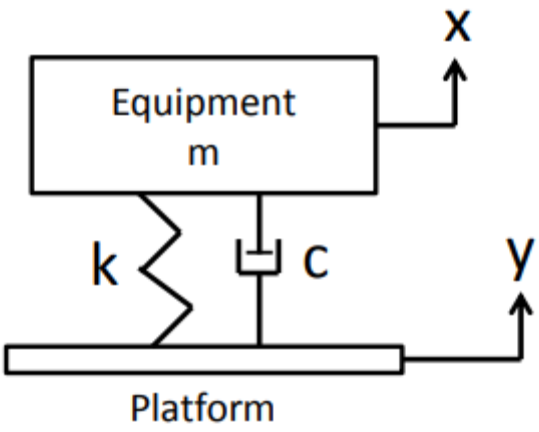

Figure 2.2 Single Degree of Freedom Voigt Model

As Kaul [31] points out, the mechanical properties of materials such as rubber are generally defined in the frequency domain. These mechanical properties are the dynamic-to-static stiffness ratio and the damping characteristics. Both factors change with excitation frequency, amplitude of loading in addition to temperature. For this reason, it is most ideal to perform experiments to obtain information on the mechanical properties of these elastomeric isolators. On the other hand, as Cinarel [32] mentions, a high number of experiments with good accuracy are needed to obtain a reliable characterization of the mechanical properties. Obtaining these results needs high cost and longer time for isolation analysis and optimization. Because of this reason, the dynamic to static stiffness ratio is assumed to be set to unity in this thesis study for simplicity. Also, since the structural damping is the most commonly used model for commercial isolators [32], instead of using viscous damping, the isolators are defined in terms of structural damping characteristics. For those types of elastomer mounts, complex spring stiffness is used to model the dynamic behavior as;

$$k^* = k(1 + i\eta) \tag{1}$$

where k is the stiffness coefficient, η is the loss factor and i is the complex number.

3. FATIGUE THEORY

3.1. Damage Theories

The main life estimation methods are Stress Life, Strain Life and Crack Propagation approaches. Both Stress-life and strain-life methods estimate the fatigue life of a part until crack initiation, and crack propagation calculates the crack growth time until fracture occurs. If the applied loads are lower than the yield strength, the most suitable method is the stress life method. On the other hand, for the loads higher than the yield strength, the strain life method is more suitable. Contrary to stress life and strain life methods, crack must have initiated in order to use crack propagation method. Also, the shape and size of the crack must be known clearly.

Vibration fatigue, one of the stress life methods, will be used in this thesis; therefore, the stress life method is explained in detail. Other methods are briefly mentioned.

3.1.1. Stress Life Approach

In order to use the stress life method, the material is assumed to be fully elastic and the applied loads are well below the yield strength.

Stress-life approach considers the ratio of maximum stress to minimum stress. Two basic stress cycles are shown in Figure 3-1. Fully reversed cycle, which is generally found for rotating components while they are working at constant speed and load can be seen in part a. Repeated stress with a positive mean can also be seen in part-b.

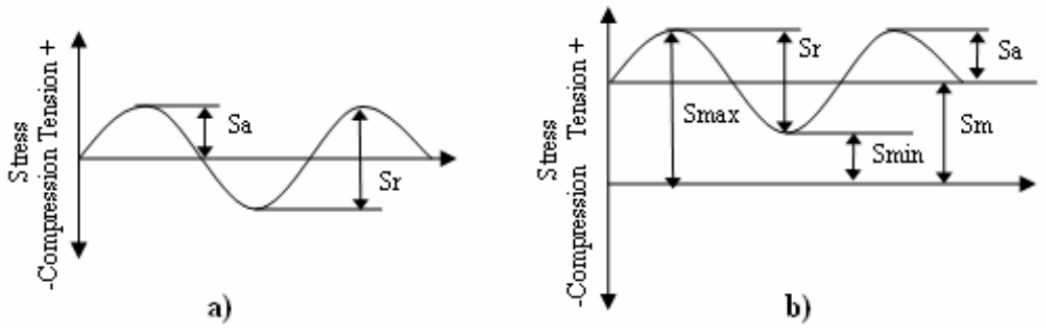

Figure 3.1 Fatigue stress cycles

Sa: Alternating stress amplitude

Sr: Stress range

Sm: Mean stress

Smax: Maximum stress amplitude

Smin: Minimum stress amplitude

R: Stress ratio, Smin/Smax

After many tests, S/N curves of the materials under cyclic loads are presented. In the graph, "S" value represents the stress amplitude and "N" indicates the number of cycles. The S/N graph is plotted in logarithmic scale, with N on the x-axis and S on the y-axis. Also, S can be graphed in linear scale. The relationship between S and N is shown below.

$$N = C.S^{-b} \tag{2}$$

Where C is related intercept on the y-axis and $-b$ is the slope of the curve. "b" also called the Basquin exponent.

In ferrous metals, the graph becomes horizontal after a certain cycle, this stress value is called the endurance limit. Infinite life is obtained if cyclic load is applied below the endurance limit. There is no endurance limit for non-ferrous metals, and the curve goes down continuously as the number of cycles increases. Around 10^8 cycles is accepted as fatigue strength of material for non-ferrous metals.

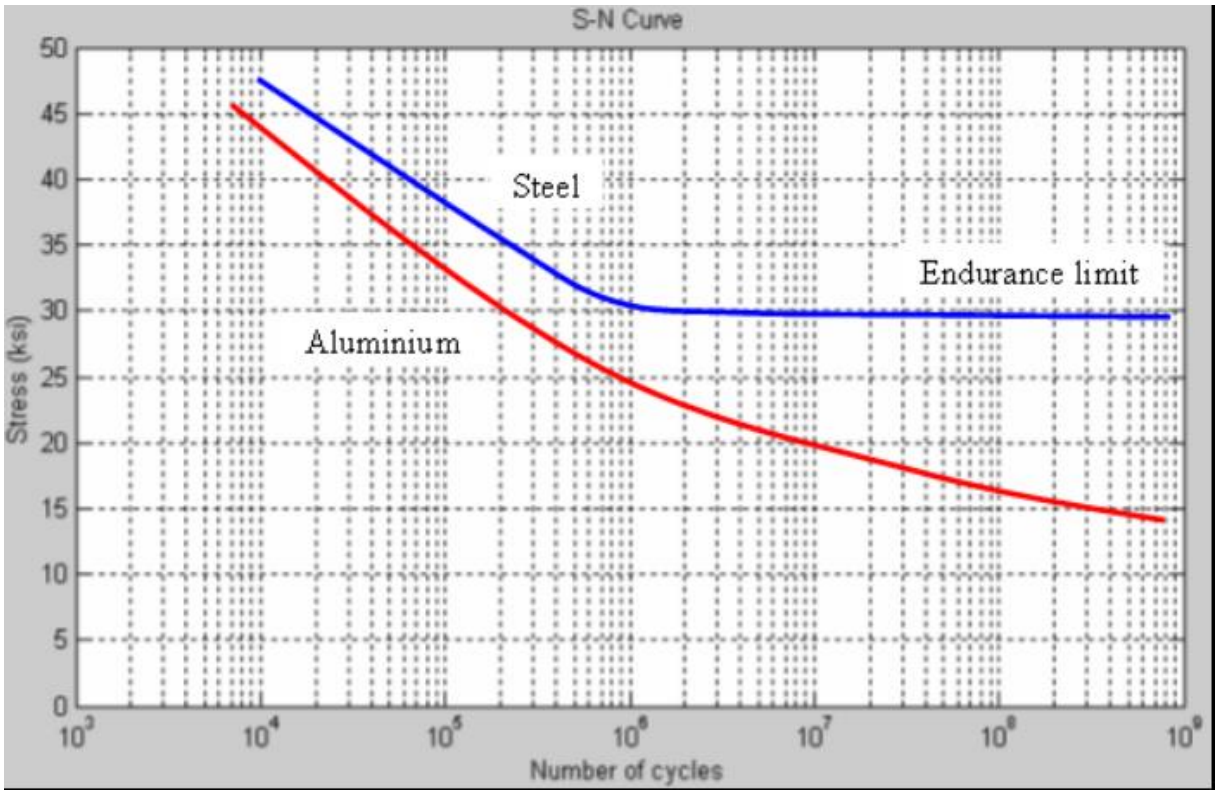

Figure 3.2 S/N curves for ferrous and non ferrous metals

Stress concentration regions on parts such as notches and holes reduce the fatigue life of the part. Therefore, sharp corners are avoided and surfaces are polished while producing the specimen. A factor is used to find the effect of stress concentration on fatigue life, called K_T. The formula for K_t is given below. [23]

$$K_t = \frac{\text{Maximum Stress in the region of the notch}}{\text{Nominal Stress away from the notch}} \tag{3}$$

Although it is not easy to calculate the stress concentration by hand, this problem can be handled with finite element method. Reduced version of K_t can be used for some materials that are not completely sensitive to notch formation. [33]

$$\sigma_{max} = K_f \sigma_0 \quad or \quad \tau_{max} = K_{fs} \tau_0 \tag{4}$$

K_f can be defined as reduced value of K_t. The notch sensitivity, q, which usually takes a value between zero and one, is given in the equation below.

$$q = \frac{K_f - 1}{K_t - 1} \quad or \quad q_{shear} = \frac{K_{fs} - 1}{K_{ts} - 1} \tag{5}$$

Another parameter to be considered in fatigue life calculations is the mean stress. Although many S/N curves are plotted for fully reversed cycle, in real life applications the mean stress is not usually zero. As the mean stress increases, the alternating stress that the system can withstand decreases. While this reduction was defined as linear by Goodman and Soderberg, it was defined as parabolic by Gerber.

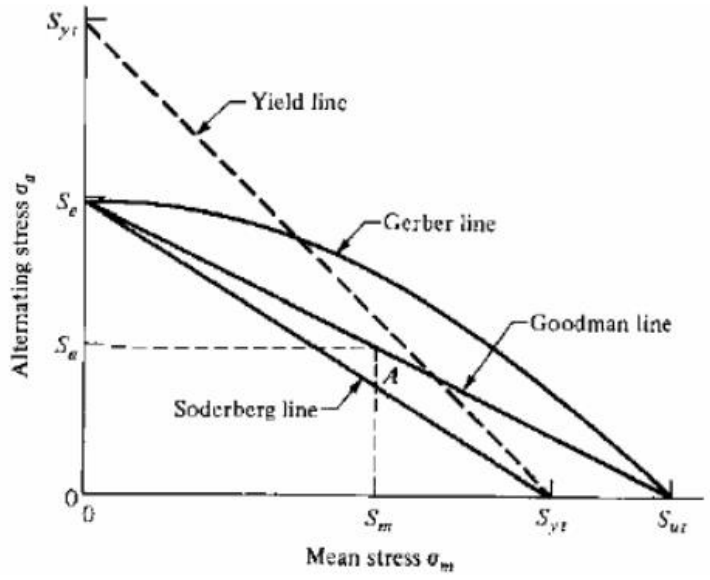

Figure 3.3 Soderberg, Goodman and Gerber approaches [33]

Goodman's Model : $\sigma_a = \sigma_0[1 - \frac{\sigma_m}{\sigma_{UTS}}]$

Soderberg's Model : $\sigma_a = \sigma_0[1 - \frac{\sigma_m}{\sigma_Y}]$

Geber's Model : $\sigma_a = \sigma_0[1 - (\frac{\sigma_m}{\sigma_{UTS}})^2]$

Until this part, calculation of fatigue caused by cyclic loading with constant amplitude and mean stress has been mentioned. But in real life, this type of loading is almost never encountered. Considering an airplane, the stresses that are likely to be encountered during its flight are as follows.

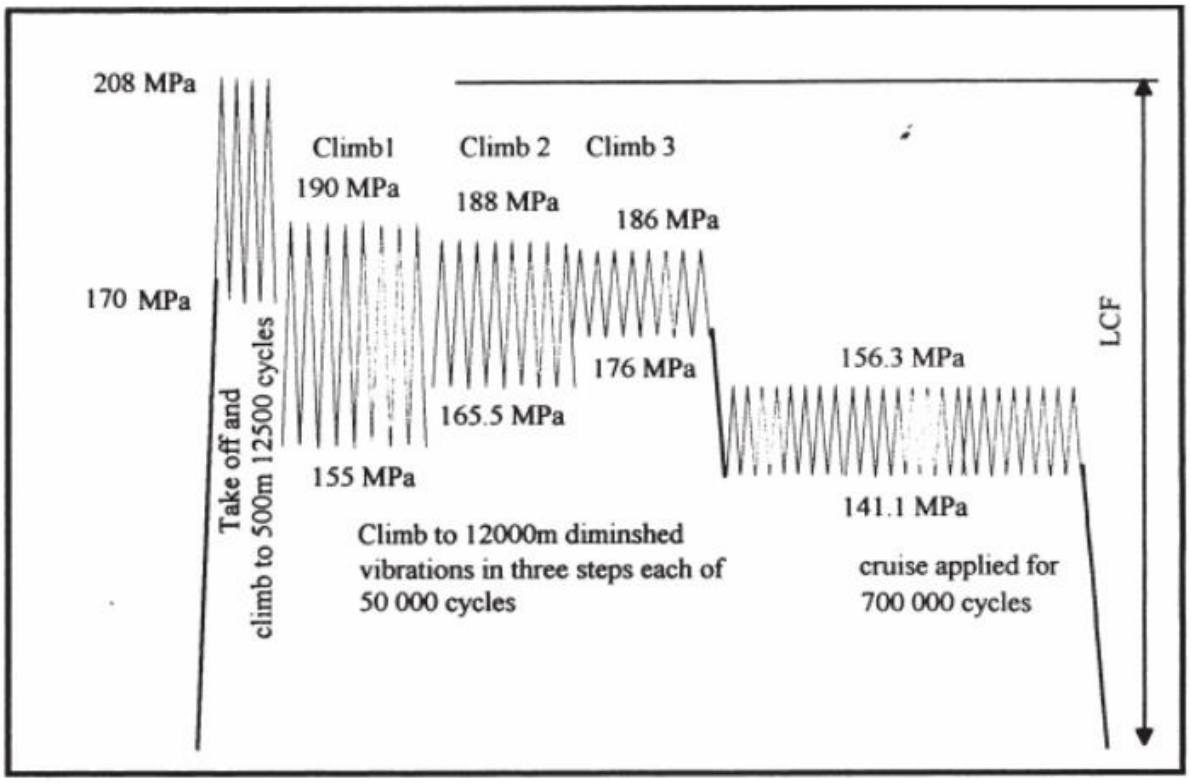

Figure 3.4 Stress cycles encountered by an airplane for different flight regimes [34]

In such a case, the damage of each cyclic load must be calculated and summed up separately. To solve this problem, Palmgren and Miner presented the following simple formula.

$$\sum_{i=1}^{k} \frac{n_i}{N_i} = [ED] \quad (6)$$

k: The number of stress cycle blocks with different amplitudes and/or means

N: The number of cycles the material can withstand at applied fixed stress amplitude

n: The number of stress cycles applied at a fixed stress amplitude

Where $[ED]$ is the total accumulated damage. When $[ED]$ is equal to one, the part is at the end of its life and it fails. For Palmgren-Miner theorem, the order of the cyclic loadings does not matter.

It is not possible to directly apply the more complex stress histories encountered in real life to the Palmgren-Miner equation. If the stress history is random, it is necessary to use a cycle counting method to find the value n. Rainflow cycle counting method is the most preferred method as it provides all the necessary information for fatigue life analysis such as the mean, amplitude and the number of repetitions [14].

Rainflow cycle counting method finds loads with the same amplitude and mean in the data and groups them. The operation procedure of the method is described in order below.

- The time and stress axes in the loading history are interchanged. The graph becomes similar to a pagoda roof after this transformation.
- The right sides of this roof are considered as peaks and the left sides as valleys.
- Two different paths are followed, depending on where the fall begins [35].
- If the fall starts from a peak;
    - The drop will stop when it reaches a higher peak than itself.
    - The drop will stop if it meets the path through which another predetermined drop passes.
    - The drop can fall to another roof and continue to slip, following the previous two rules.
- If the fall starts from a valley;
    - The drop will stop when it reaches a deeper valley than itself.
    - The drop will stop if it meets the path through which another predetermined drop passes.
    - The drop can fall to another roof and continue to slip, following the previous two rules.

The following example is given to explain the above algorithm better.

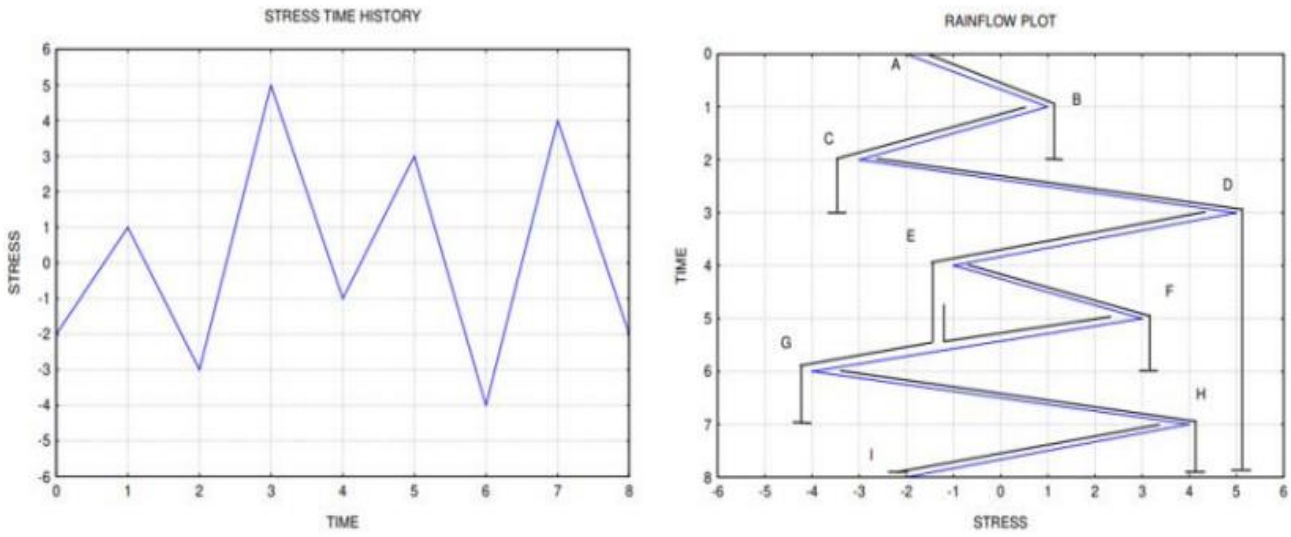

Figure 3.5 Rainflow cycle counting method [36]

Table 3-1 The output of a rainflow cycle counted data [36]

Path	Cycles	Stress Range	Peak	Valley	Mean
A-B	0,5	3	1	-2	-0,5
B-C	0,5	4	1	-3	-1
C-D	0,5	8	5	-3	1
D-G	0,5	9	5	-4	0,5
E-F	1	4	3	-1	1
G-H	0,5	8	4	-4	0
H-I	0,5	6	4	-2	1

The output of stress-time data by the Rainflow cycle counting method is usually a range-mean histogram. The stress range, mean and cycle informations that are required for the Palmgren-Miner theorem is obtained by the cycle counting method.

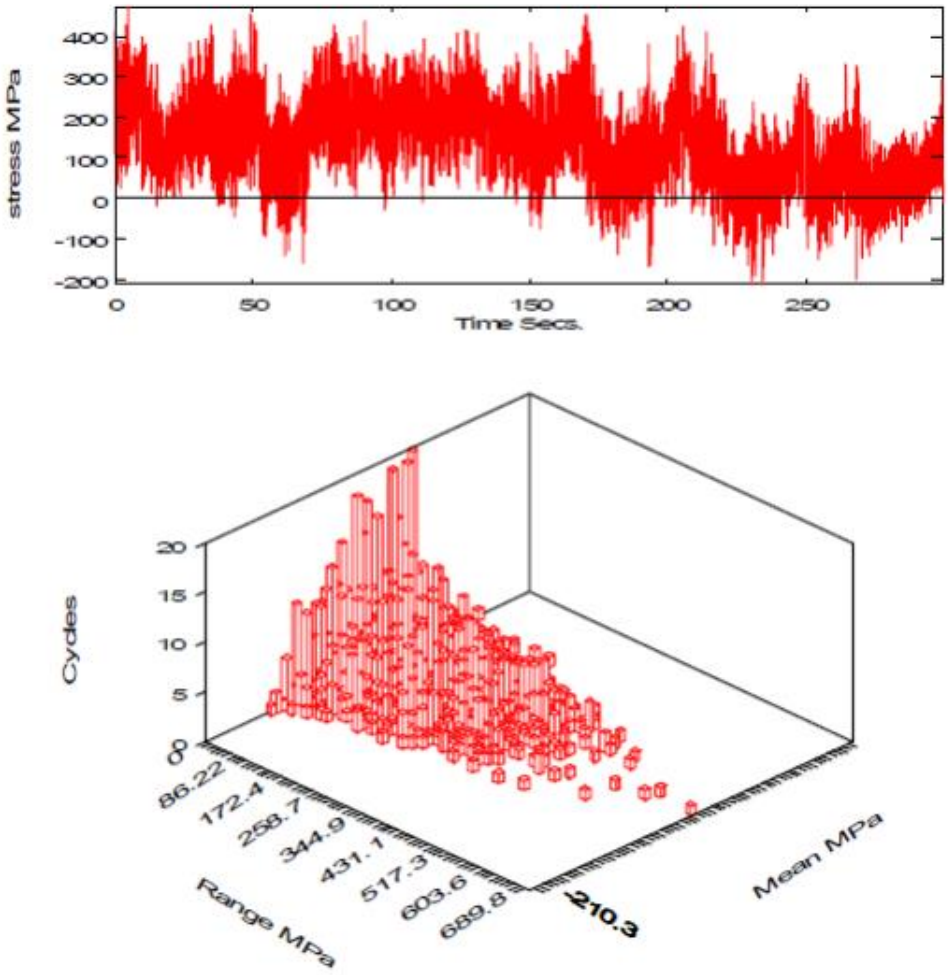

Figure 3.6 Range-Mean Histogram of rainflow cycle counted data [37]

The Stress Life method focuses on the equivalent stress of a particular point on the part. On the other hand, this stress occurs as a combination of the whole stresses at stated point. In order to obtain accurate results, it is important to choose the appropriate combination method to reduce the stresses in different axes to a single axis.

Three-dimensional stress tensor with nine components is used to indicate the stress state on the part. 3D stress tensor can be reduced to three principal stresses and their directions.

$$\begin{bmatrix} \sigma_{xx} & \sigma_{xy} & \sigma_{xz} \\ \sigma_{xy} & \sigma_{yy} & \sigma_{yz} \\ \sigma_{xz} & \sigma_{yz} & \sigma_{zz} \end{bmatrix} = \begin{bmatrix} \sigma_1 & 0 & 0 \\ 0 & \sigma_2 & 0 \\ 0 & 0 & \sigma_3 \end{bmatrix} \tag{7}$$

Usually, fatigue crack initiates at free surfaces where the shear and normal stresses are zero or the sheet is thin enough so the principal stress normal to the surface is indicated with $\sigma_3 = 0$.

The two remaining principal stresses are designated as σ_1 and σ_2, respectively, in order of magnitude.

It is important to determine whether systems with two or more excitation load inputs are proportional or non-proportional to decide the appropriate method.

Two parameters used for determining the multiaxiality condition are defined as follows:

Biaxiality Ratio $$\alpha = \frac{\sigma_2}{\sigma_1} \quad (7)$$

Principal Stress Angle φ: Angle between σ_1 and x-axis

where;

σ_1, σ_2: Principal stresses.

If the biaxiality ratio, α, and principal stress angle, φ, remain constant under variable loads, it is considered as proportional multiaxial loading, if not, it is considered as non-proportional multiaxial loading.

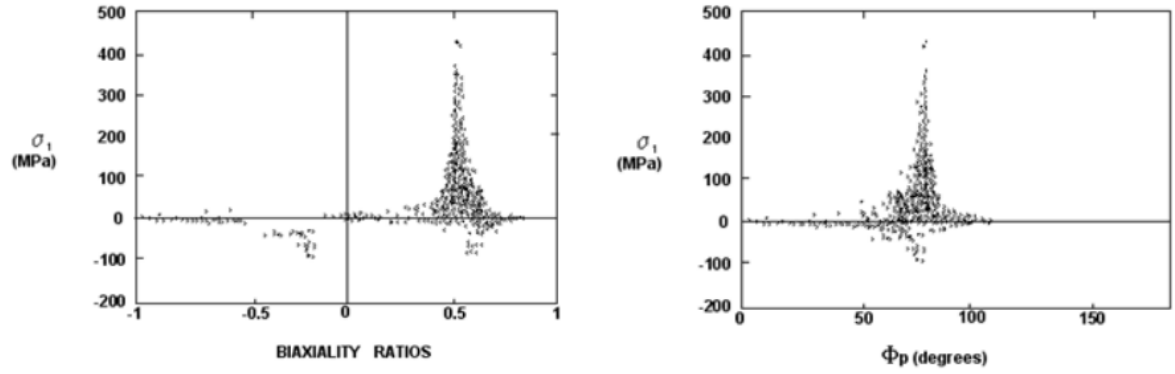

Figure 3.7 Principal Stress vs biaxiality ratio and principal stress angle for multiaxial proportional loadings [38]

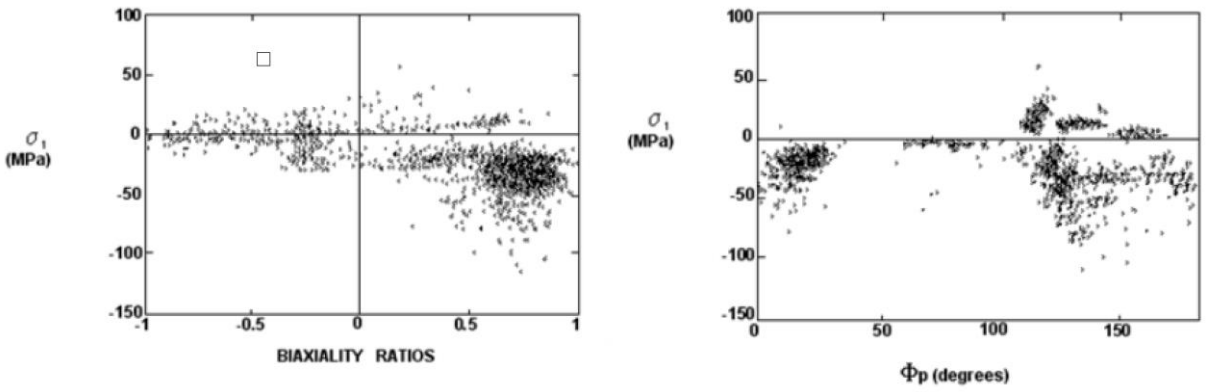

Figure 3.8 Principal Stress vs biaxiality ratio and principal stress angle for multiaxial non-proportional loadings [38]

Combination methods according to proportionality by using principal stress angle and biaxiality ratio can be selected as follows.

Table 3-2 Combination methods according to proportionality [23]

Stress State	**Principle Stress Angle, φ**	**Biaxiality Ratio, α**	**Combination Method**
Uniaxial	Constant	$\alpha = 0$	Uniaxial Theories
Proportional Multiaxial	Constant	$-1 < \alpha < 1$	Equivalent StressStrain Theories
Non-proportional Multiaxial	May vary	α, May vary	Critical Plane etc

For proportional loadings, equivalent stress-strain theories can be used. These theories just sum the damage regardless of whether the principals stress directions change. Therefore, it is not suitable to be used in non-proportional loads. For non-proportional loadings, the critical plane method calculates the fatigue damage for all possible planes and the most damageable plane, which is the critical plane, is chosen.

Different stress representations of a cylindrical notched specimen with an axial sine loading are shown below.

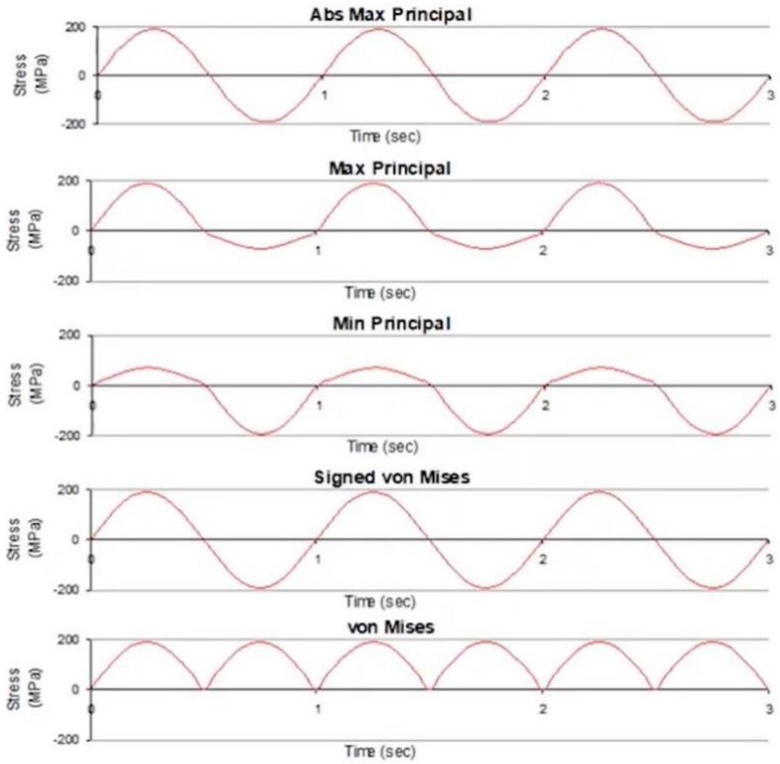

Figure 3.9 Equivalent stress theories for a cylindrical notched specimen with uniaxial sine loading [39]

Absolute maximum principal stress theory is described as the principal stress with the largest magnitude and its sign.

$$\sigma_{AMP} = sign * \sigma_{AMP} \tag{8}$$

Where,

$$\sigma_{AMP} = \max(|\sigma_1|, |\sigma_2|, |\sigma_3|) \tag{9}$$

Signed Von Misses criterion is the Von Mises stress but forced to take the sign of absolute maximum principal stress.

$$\sigma_{SVM} = \frac{\sigma_{AMP}}{|\sigma_{AMP}|} \cdot \sqrt{\frac{(\sigma_1-\sigma_2)^2+(\sigma_2-\sigma_3)^2+(\sigma_3-\sigma_1)^2}{2}} \tag{10}$$

3.1.2. Strain Life Approach

Plastic deformation, which leads the structure to have a shorter life than the design specification, can occur if the cyclic loads are relatively large. When plastic deformation occurs in a component, Strain-Cycle curve should be used instead of S/N curve to obtain fatigue life [40].

3.1.3. Crack Propagation Approach

Both stress and strain life theories are valid until the crack begins. The crack propagation approach, on the other hand, calculates the time from crack initiation to fracture. For this theory, the shape and size of the crack is known.

3.2. Random Vibration Fatigue

The methods mentioned so far are time-domain methods, but the random vibration fatigue method is in the frequency-domain. Vibration fatigue approach is used when the input loading or the stress history obtained from the structure is random in nature. Hence, this approach is the best specified using statistical information about the process [24].

Frequency response functions are used to obtain the response of the structure to the random loading.

$$Response(f) = H(f) \times Input(f) \tag{11}$$

Where,

$Response(f)$: Response FFT of the system

$H(f)$: Frequency response function of the system

$Input(f)$: Input FFT to the system

Frequency response function of a system can be obtained by modal and harmonic analyses using the finite element method. Thus, the dynamic stresses of the system can be reached for the given load input by using Equation (11). Note that this method takes the dynamics of the system (natural frequencies and mode shapes) into account as opposed to calculating static stresses.

Miner's linear damage accumulation model and S/N diagram equation is represented in random vibration theory as follows [41].

$$E[D] = E[P]\frac{T}{C}\int_0^\infty S^b p(S)\, dS \tag{12}$$

Where,

$E[D]$: Expected value of damage

$E[P]$: Expected number of peaks per second

T: Life in seconds

C: Material constant from S/N equation

b: Inverse slope of the Woehler curve

S: Stress amplitude

$p(S)$: Probability density function of Rainflow stress ranges

If the $E[D]$ value in Equation (12) is set to 1, the fatigue life, T, in seconds is obtained. There are many empirical solutions to the Probability Density Function of Rainflow stress ranges, p(S), like Tunna, Wirsching, Hancock, Chaudhury and Dover. However, the best correlation was obtained by Dirlik after extensive computer simulations to model random signals thanks to the Monte Carlo method [42].

$$p(S_i) = \frac{\frac{D_1}{Q}e^{\frac{-Z_i}{Q}} + \frac{D_2 Z_i}{R^2}e^{\frac{-{Z_i}^2}{2R^2}} + D_3 Z_i e^{\frac{-{Z_i}^2}{2}}}{2\sqrt{m_0}} \quad (13)$$

Where,

m_i: i^{th} moment of stres PSD

$$Z_i = \frac{S_i}{2\sqrt{m_0}}, \qquad \gamma = \frac{E[0]}{E[P]}, \qquad E[0] = \sqrt{\frac{m_2}{m_0}}, \qquad E[P] = \sqrt{\frac{m_4}{m_2}}, \qquad x_m = \frac{m_1}{m_0}\sqrt{\frac{m_2}{m_4}}$$

$$D_1 = \frac{2(x_m - \gamma^2)}{1 + \gamma^2}$$

$$D_2 = \frac{1 - \gamma - D_1 + {D_1}^2}{1 - R}$$

$$D_3 = 1 - D_1 - D_2$$

$$Q = \frac{1.25(\gamma - D_3 - D_2 R)}{D_1}$$

$$R = \frac{\gamma - x_m - {D_1}^2}{1 - \gamma - D_1 + {D_1}^2}$$

4. FLIGHT DATA ACQUSITION

For the fatigue analysis to give more realistic results, flight tests were performed to obtain vibration data from the aircraft. In the flight tests, data were collected during all maneuvers and flight conditions of the aircraft, and these data were then synthesized. The durations of the flight conditions and the values of PSD graphs are not given due to military confidentiality.

Table 4-1 Flight Conditions and Durations

Condition No	Flight Condition	Duration [h]	Life Duration [h]
1	Ground Idle	t_1	$T_1 = T_{total} * \left(\frac{t_1}{t_{total}}\right)$
2	Ground Max Rotor RPM	t_2	$T_2 = T_{total} * \left(\frac{t_2}{t_{total}}\right)$
3	Climbing	t_3	$T_3 = T_{total} * \left(\frac{t_3}{t_{total}}\right)$
4	Cruise Speed	t_4	$T_4 = T_{total} * \left(\frac{t_4}{t_{total}}\right)$
5	Max Speed	t_5	$T_5 = T_{total} * \left(\frac{t_5}{t_{total}}\right)$
6	Sharp Turn	t_6	$T_6 = T_{total} * \left(\frac{t_6}{t_{total}}\right)$
7	Hover IGE	t_7	$T_7 = T_{total} * \left(\frac{t_7}{t_{total}}\right)$
8	Hover OGE	t_8	$T_8 = T_{total} * \left(\frac{t_8}{t_{total}}\right)$
9	Hover Turn	t_9	$T_9 = T_{total} * \left(\frac{t_9}{t_{total}}\right)$
10	Descend and Landing	t_{10}	$T_{10} = T_{total} * \left(\frac{t_{10}}{t_{total}}\right)$
	Total Flight Duration	$t_{total} = \sum_{i=1}^{11} t_i$	$T_{total} = 2500\ h$

During a usual mission flight of the aircraft, each phase should last for a certain duration under standard circumstances. It is denoted by t_i where i corresponds to each phase and the duration of the phases corresponds to whole operational life is indicated by T_i . In accordince with MIL-STD-810G, 2500 hours of flight duration is sufficient to simulate the total time the aircraft will fly during its lifetime. That is why T_{total} is assumed to be 2500 hours.

The operational flight data, acquired from the platform of each condition, can be combined to obtain a single PSD data as specified by the equation given below according to the MIL-STD-810G Method 514.6 Annex A [43].

$$T_{total}{G_{total}}^{m/2} = T_1{G_1}^{m/2} + T_2{G_2}^{m/2} + \cdots + T_N{G_N}^{m/2} \quad (14)$$

Where T_1, T_2, T_N are the time durations of each phase given in Table 4-1, G_1, G_2, G_N is the PSD value of each phase. It suggests taking "m" as 80 percent of the slope of S/N curve for random waveshapes. Historically m = 7.5 has been used for random environments but the values between 5 and 8 are also frequently used [43].

The data sampling frequency is 8000 Hz. Collected vibration data is converted to g from mV using reference sensitivities in the sensor manuals. These data in the time domain are transformed into the frequency domain by Welch's power spectral density estimates. The transformation is done with the “pwelch” command in Matlab. The PSD is obtained up to 4000 Hz due to the Nyquist theorem and the frequency resolution of the PSD data is set to 0.244 Hz. For each axis 2500 hours of acceleration PSDs which were obtained from flight tests are provided in Figure 4.1.

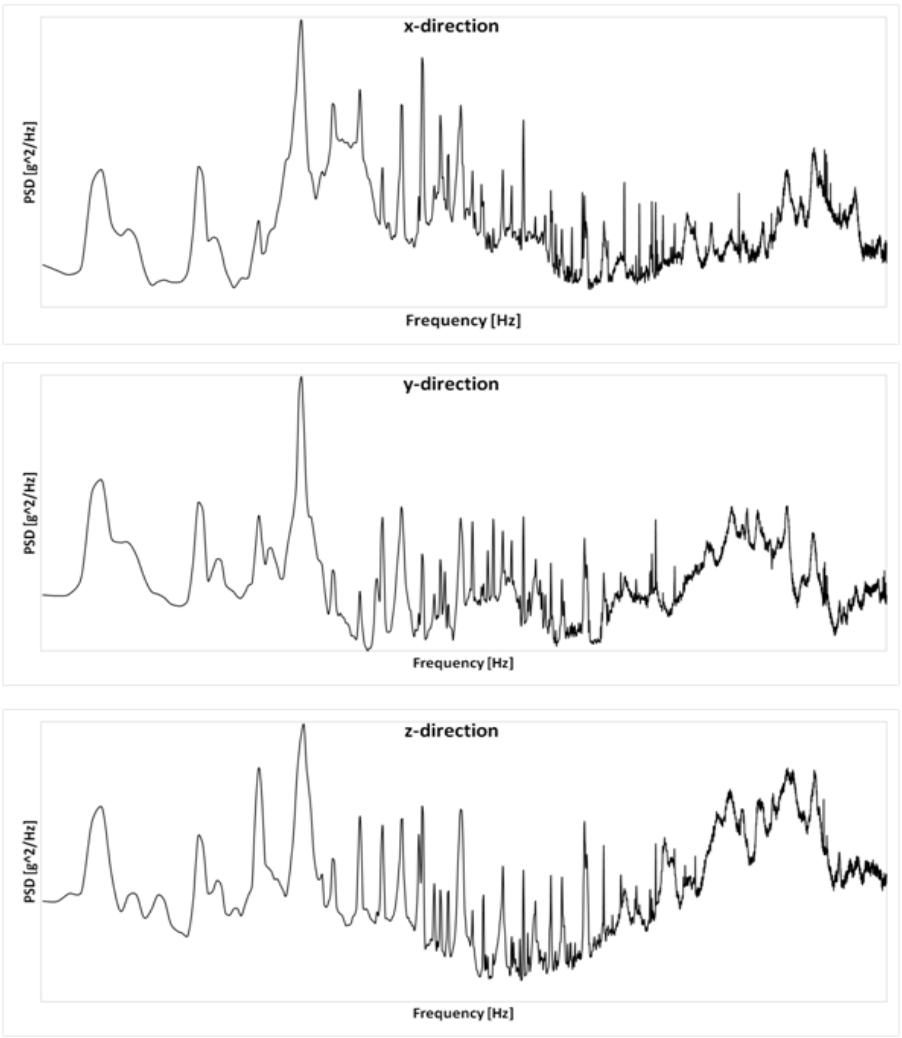

Figure 4.1 Acceleration PSD’s

Since the loading conditions are multiaxial, the multiaxial theory should be applied. On the other hand, in this study, since the electromagnetic shaker system is not capable of providing simultaneous multi-axis loading, all analyzes will be carried out with single axis acceleration PSD input so that the analyzes can be verified by experiments. An enveloping method is preferred to be on the safe side. To obtain a single axis acceleration PSD, maximum value at each frequency of each direction is used.

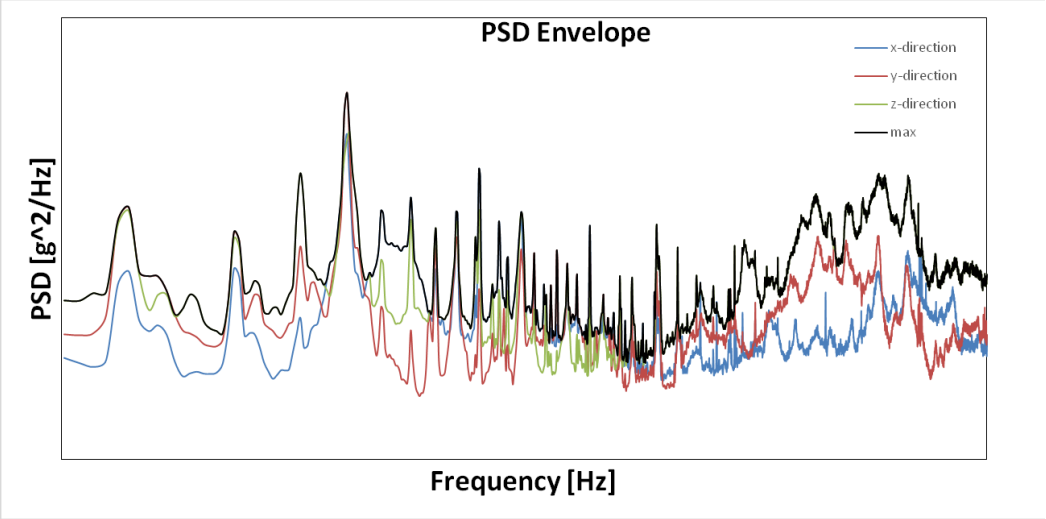

Figure 4.2 PSD Envelope

Vibration data that were obtained from the aircraft were taken only once. The reason for this is that all measurements to be made have the same mean value because the vibration characteristic is ergodic random. Ergodic random process means that the time averages of the process tend to be the appropriate ensemble averages. This shows that the PSD graph to be created will not change even if the measurements are repeated.

The 2500-hour period, which represents the platform's entire lifetime, is used to obtain the lifetime of the components in finite element analysis. On the other hand, an experimental fatigue analysis with 2500 hours of data is not possible. As a result, by accelerating 2500 hours of PSD data into 4 hours with same damage values at the end of the duration, the analysis can be possible. Then, the equation from MIL-STD-810G Method 514.6 Annex A is used as follows,

$$T_4 {G_4}^{m/2} = T_{2500} {G_{2500}}^{m/2} \tag{15}$$

Here, G_4 is the 4 hours PSD, G_{2500} is the enveloped 2500 hours PSD, T_{2500} is 2500 hours, T_4 is 4 hours and m is the scaling factor. The value of m is 7.5, which is the suggested value in the standard for random environments.

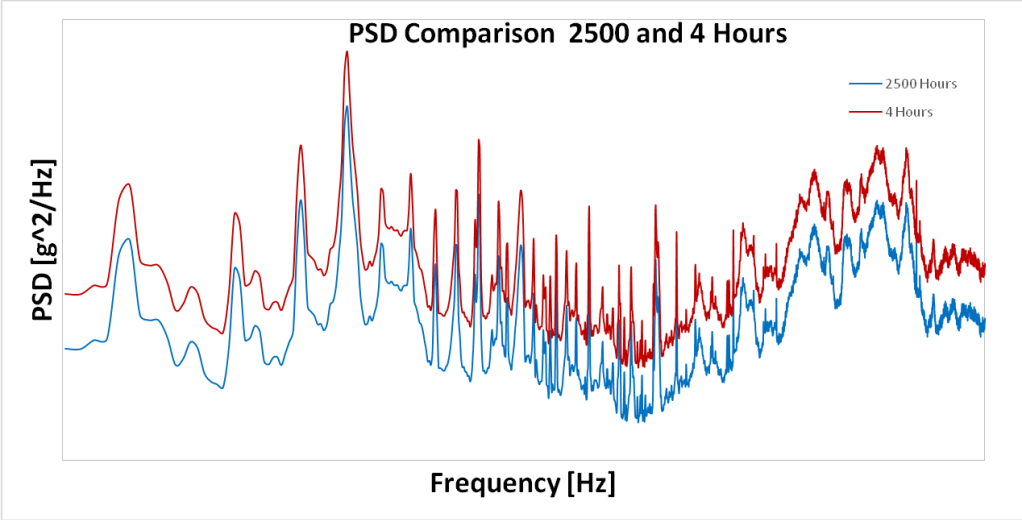

Figure 4.3 PSD Comparison for 2500 and 4 Hours

5. VIBRATION FATIGUE ANALYSIS AND VERIFICATION

5.1. Finite Element Model Preparation

Since the finite element model directly affects the result of the fatigue analysis, it needs to be carefully prepared. The avionics unit contains many electronic boards and components and each of them have their own natural frequencies. In order not to see peaks at these frequencies in the verification tests, the avionic unit is modeled as an aluminum block with equivalent weight.

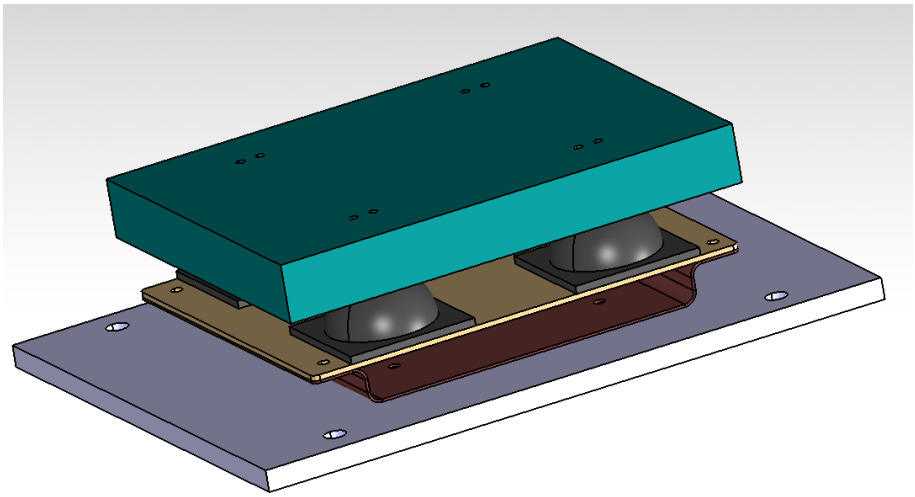

Figure 5.1 CAD Model of Test Setup

In finite element analysis, thin-walled structures are modeled with shell elements to increase computational efficiency. For sheet metal parts whose thickness is lower compared to their large surface area, a mid-surface is formed. After this process, two-dimensional surfaces are

created geometrically, and then the analysis model is prepared by creating a mesh structure on this surface.

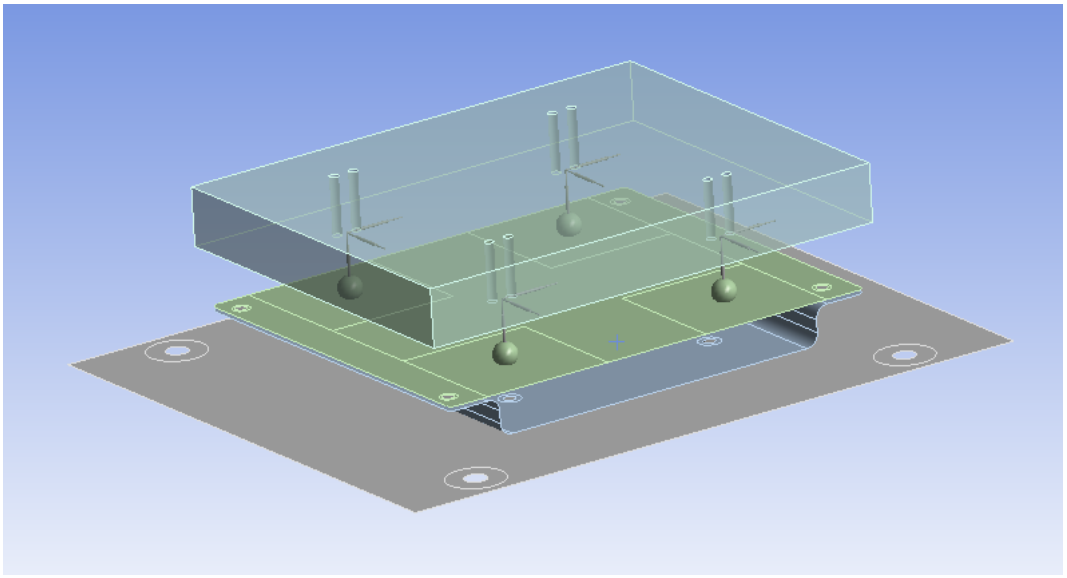

Figure 5.2 Simplified ANSYS Model

The shock absorbers are modeled as 3-axis springs and their weights are added as point masses. In this thesis, the absorbers is studied only as an element that changes the dynamic characteristics of the structure. The life of the absorber was not investigated. It has been assumed that the performance of the absorber does not change with factors such as temperature, abrasion, etc. throughout the tests and analyzes.

Aluminum 6061 T6 is assigned to the avionics unit and its tray, and Aluminum 2024 T3 is assigned to the mount. All materials was selected from nCode material library which provides S/N curves of the materials.

The aluminum block that represents the avionics unit is roughly meshed, since the meshing of the block has a insignificant result on the modes of the mount. On the other hand, adjustments have been made to improve the quality of the mesh of other parts. Sizing of the mesh continuously decreased until the stress value does not change. This method, called mesh convergence analysis, provides the required accuracy with the minimum number of mesh and shows whether there is singularity or not.

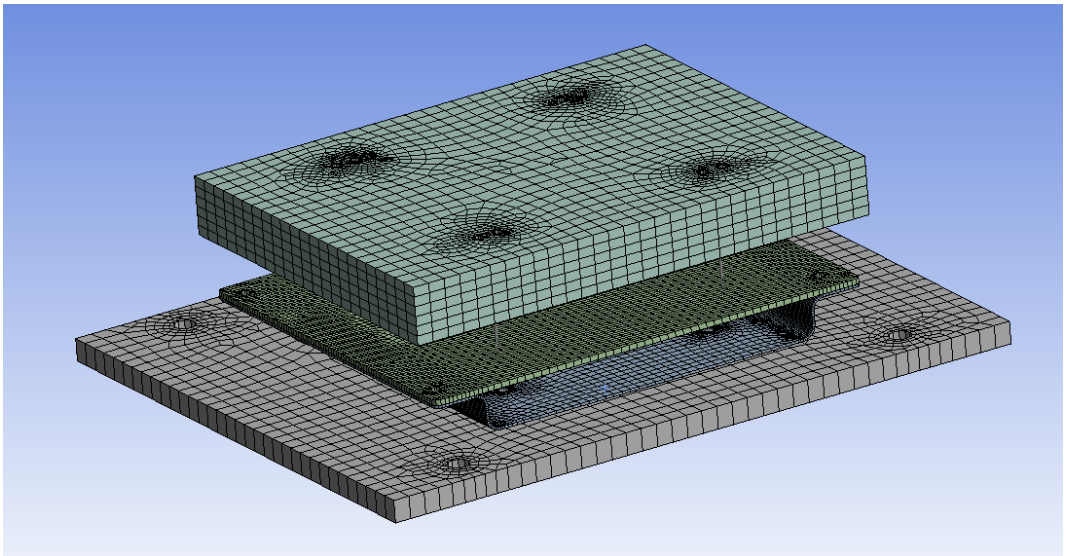

Figure 5.3 Meshed Model

5.2. Absorber Model

In the analysis, 3-axis spring connection is used to model the dynamic characteristic of the absorber. A test was performed in 3 axes with a electromagnetic shaker to obtain the stiffness and damping values of the spring connection. The test were performed with 0.002 g^2/hz white noise and 4 accelerometer were used to obtain the response of the structure.Only shock absorbers and block are used in this test.

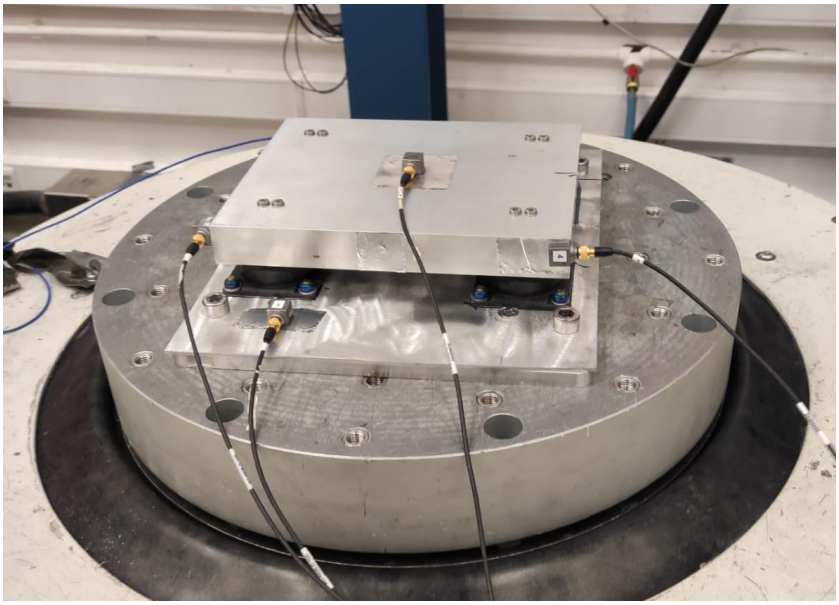

Figure 5.4 Test for Obtaining the Absorber Characteristics

The stiffness and damping values were obtained using the test results. According to the test, stiffness of the absorbers is 8700 N/m in 3 axis and the damping ratio is 0.17. The damping

ratio was calculated using the half-power bandwidth method. These values were used in the spring connection and the analysis results were compared with the test results.

Direction	Experiment Natural Frequency [Hz]	Analysis Natural Frequency [Hz]	Damping Ratios
x	16.1	15.9	0.14
y	17.6	16.9	0.13
z	16.5	16.5	0.17

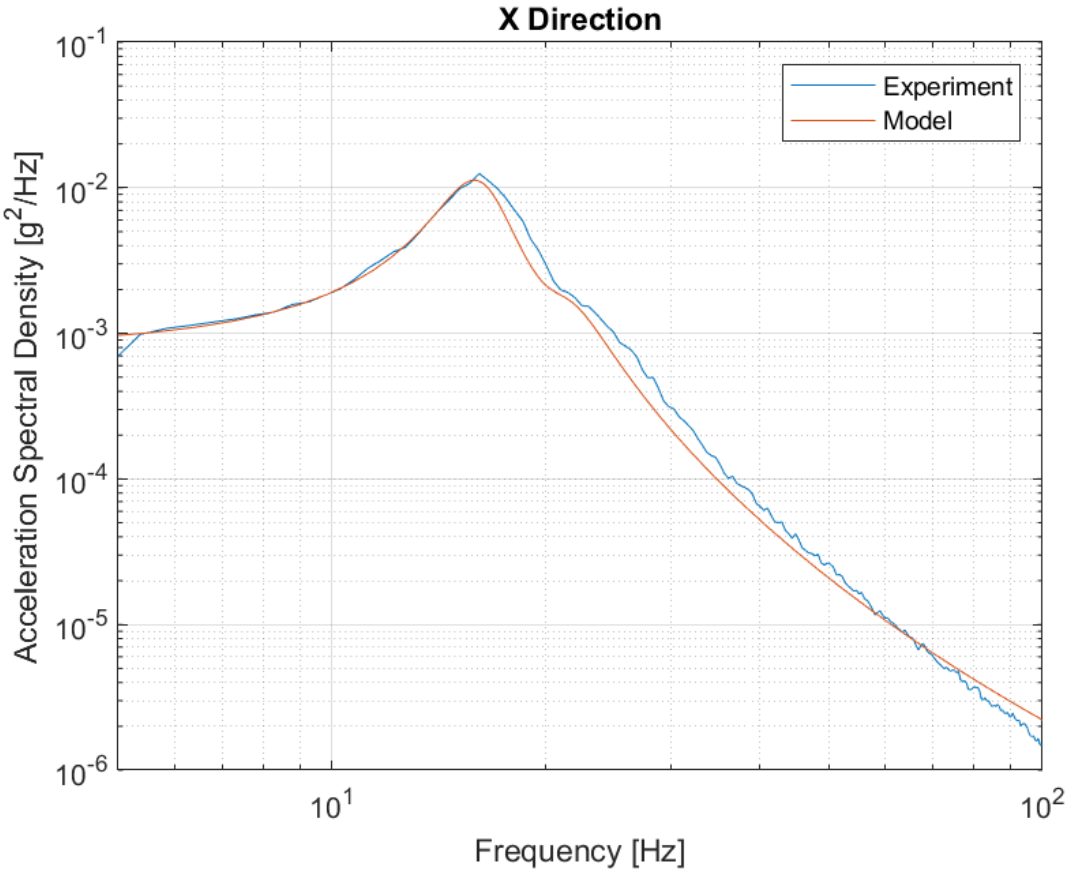

Figure 5.5 PSD Comparison for Model and Test Results in X-Direction

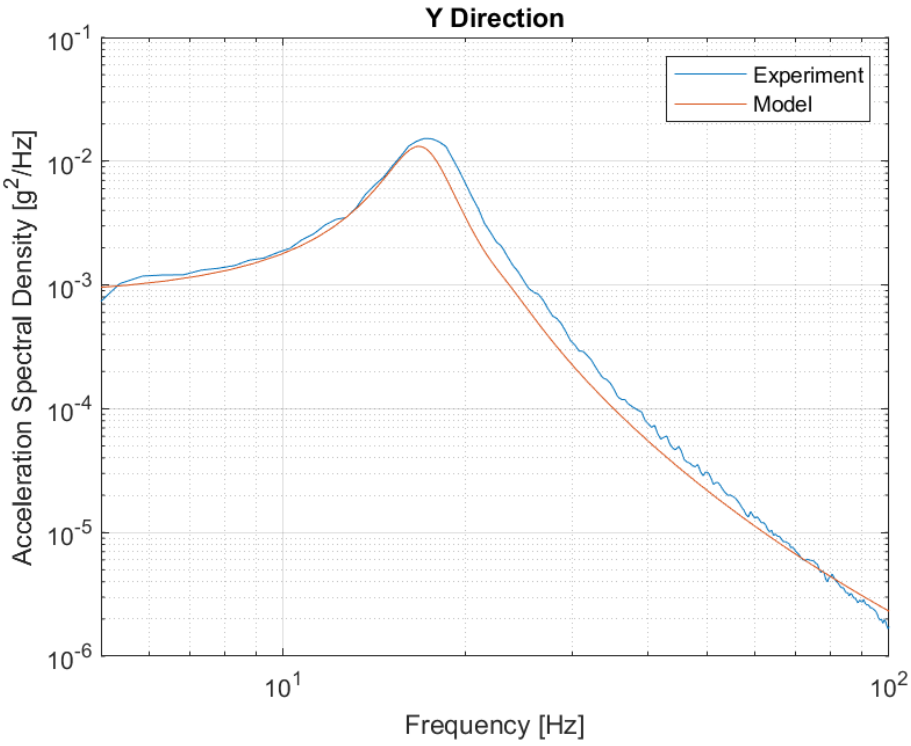

Figure 5.6 PSD Comparison for Model and Test Results in Y-Direction

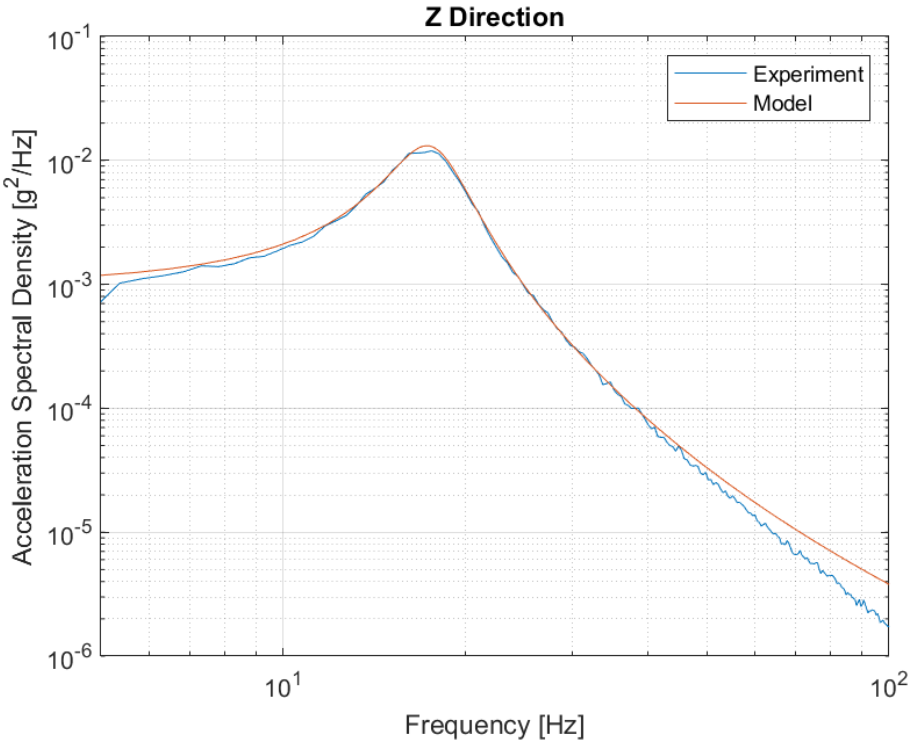

Figure 5.7 PSD Comparison for Model and Test Results in Z-Direction

The experiment was repeated in z axis at different amplitudes to understand whether the absorber works linearly. The transmissibility plots of the tests and damping ratios are given below.

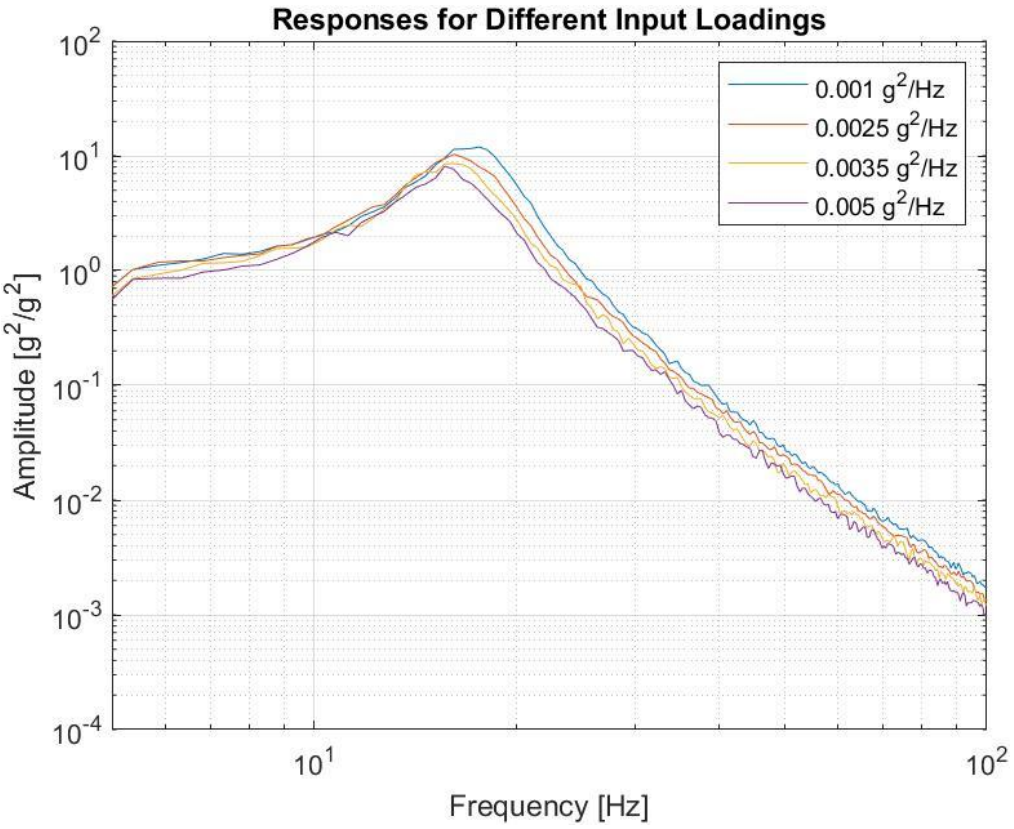

Figure 5.8 Responses for Different Input Loadings

Table 5-1 Experiment Amplitudes and Corresponding Damping Ratios

Experiment Amplitude [g^2/Hz]	Damping Ratio
0.001	0.16
0.0025	0.17
0.0035	0.17
0.005	0.16

Table 5-1 shows that, with changing input amplitude natural frequency of the absorber change slightly. The damping ratios also do not change much. It can be assumed that there isn't a non-linearity in the absorber dynamics.

5.3. Finite Element Model

After the verification of the absorber models, the model of the whole system was prepared. All bolts in the system are modelled with deformable structural steel beam element. Changing contact types and contact areas changes the natural frequencies as well. Therefore, modal testing was performed to determine the correct type of contact and the diameter of the contact area.

In order to test the precision of the FEM and to determine the damping ratios, random vibration analysis and test with 0.002 g^2/hz white noise were performed and the results were compared. Damping ratios were calculated using the half-power bandwidth method.

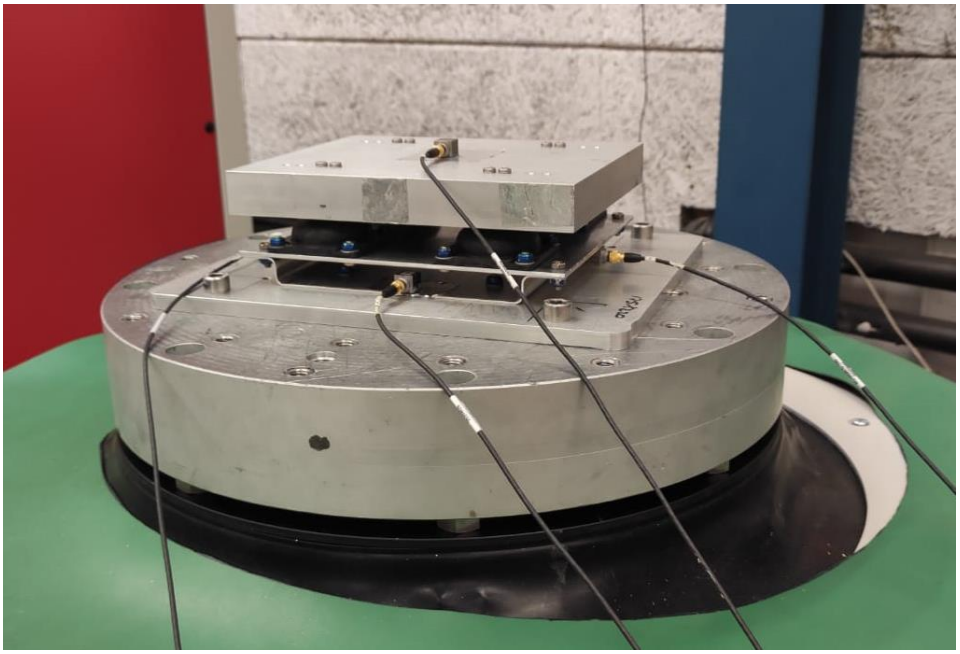

Figure 5.9 White Noise Vibration Test

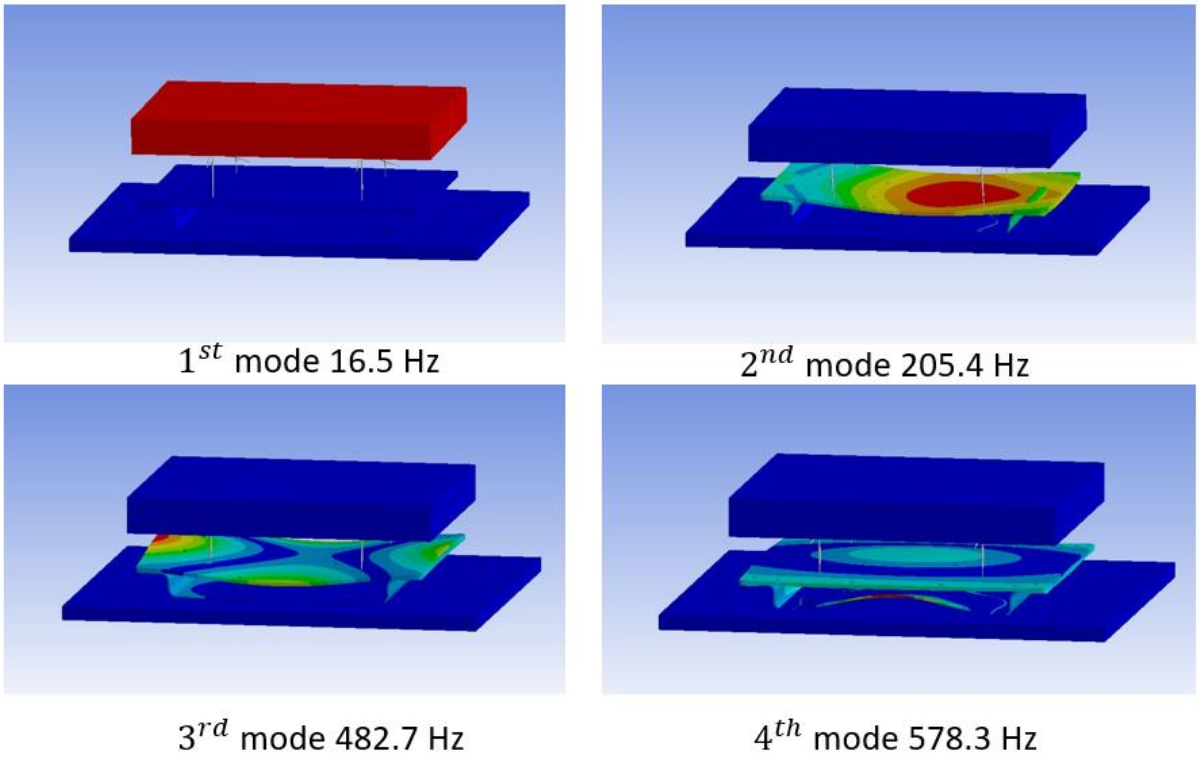

Figure 5.10 Mode Shapes of Structures

The comparison of analysis and test results is given below.

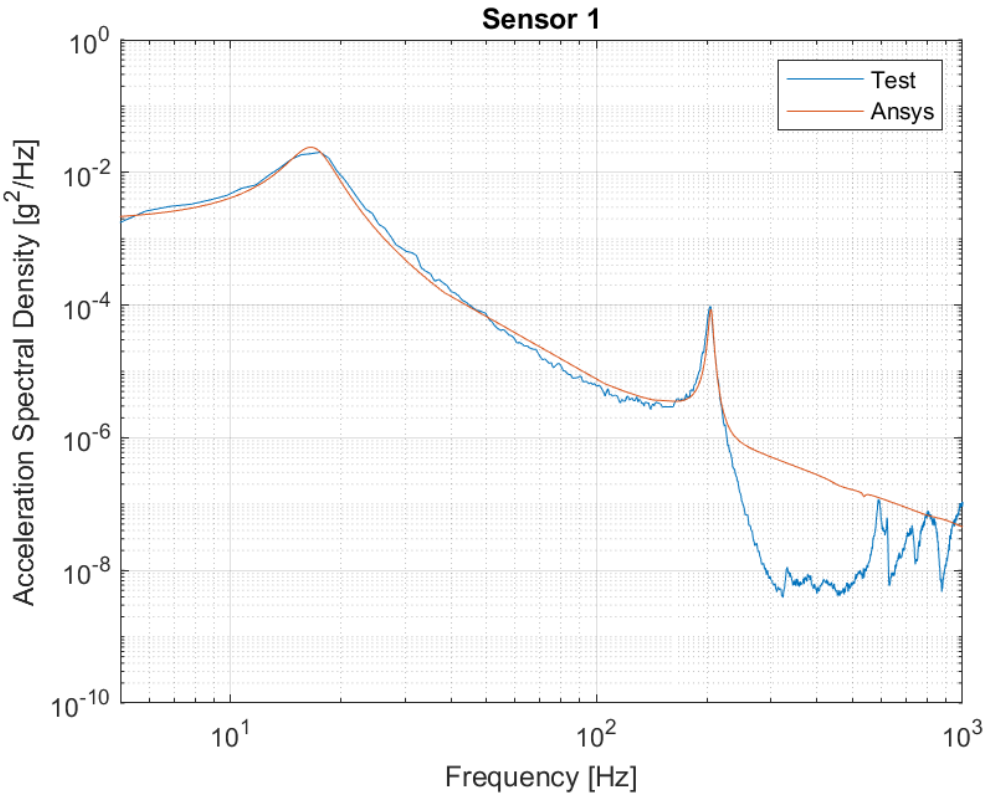

Figure 5.11 Sensor 1 Test vs ANSYS Comparison

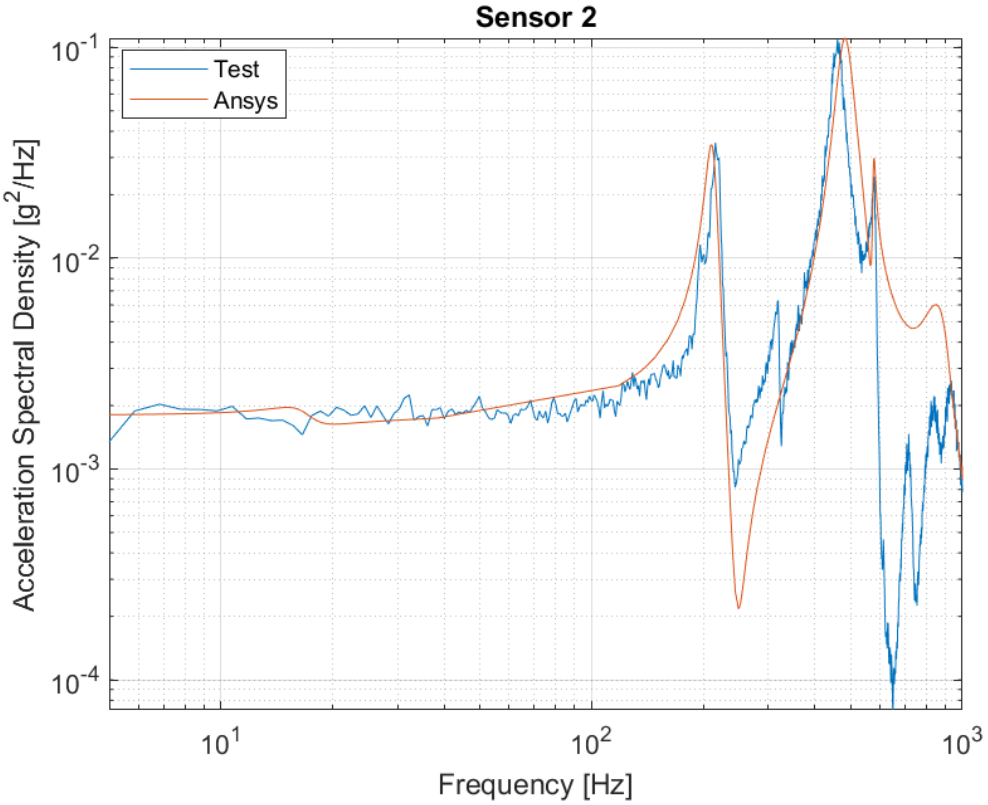

Figure 5.12 Sensor 2 Test vs ANSYS Comparison

In Table 5-2, natural frequencies acquired from the tests and finite element model and their corresponding damping ratios are given. Comparison shows that the first four natural frequencies acquired from tests and finite element model are very close to each other.

Table 5-2 Comparison of Natural Frequencies and Damping Ratios

Mode Number	Experiment Natural Frequency [Hz]	Analysis Natural Frequency [Hz]	Damping Ratios
1	16.6	16.5	0.17
2	204.1	205.4	0.015
3	460.9	482.7	0.039
4	578.1	578.3	0.018

nCode gets the FRF data from harmonic analysis. Therefore finite element model was used for mode superposition harmonic analysis which uses natural frequencies obtained by modal analysis. 1g acceleration load is used to be compatible with power spectral density.

5.4. Fatigue Life Analysis

ANSYS Random Vibration Analysis can not work with the damping coefficient written in the spring connection. The damping ratio can be inputted into the analysis settings, but in this case damping is applied to the whole structure. MSUP harmonic analysis can use this damping coefficient with the reduced damped solver. nCode takes FRF data from harmonic analysis, so it is more suitable for fatigue life analysis of the structure.

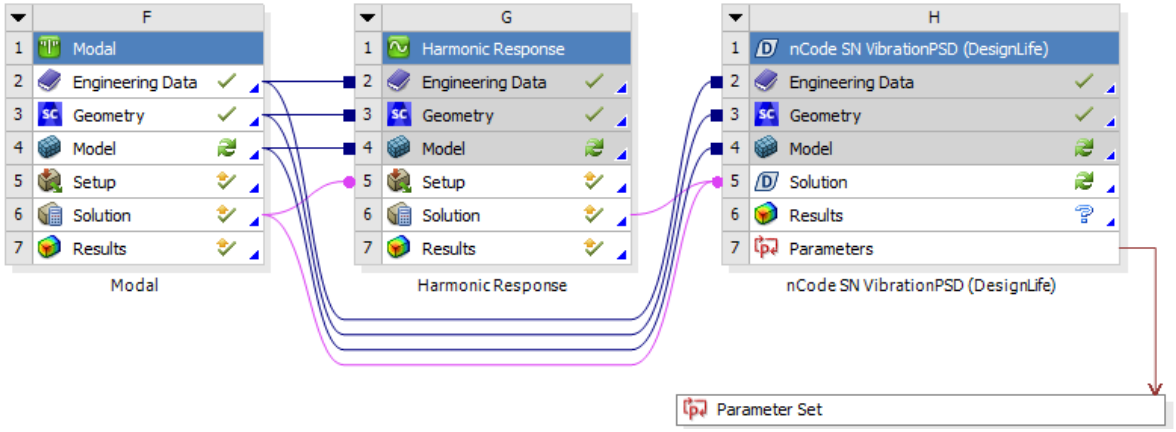

Figure 5.13 ANSYS Workbench – Ncode analysis construction

nCode has its own material library and the parts to be analyzed must be selected from this library. nCode uses glyphs for solvers, functions, inputs, and outputs. PSD data is given into the Vibration Generator glyph as an Excel spreadsheet.

nCode can perform analysis with Lalanne, Dirlik, Narrow Band and Steinberg methods. The Steinberg method was not used in the analysis because it focused on electronic components. The other three methods were used to find the fatigue life, and the results were compared with each other.

In the comparison made in Table 5-3, the damages caused by the input PSD in one second and fatigue lives are given. The value of RMS Stress is the same for all methods as it is not dependent on the cycle counting method.

Table 5-3 Fatigue Life Analysis Results for 2500 Hours PSD

Cycle Counting Method	RMS Stress [Mpa]	Damage	Life [s]	Life [h]
Lalanne	12.8	1.602e-12	6.242e+11	1.734e+08
Dirlik		1.788e-12	5.593e+11	1.554e+08
Narrow Band		3.170e-12	3.155e+11	8.764e+07

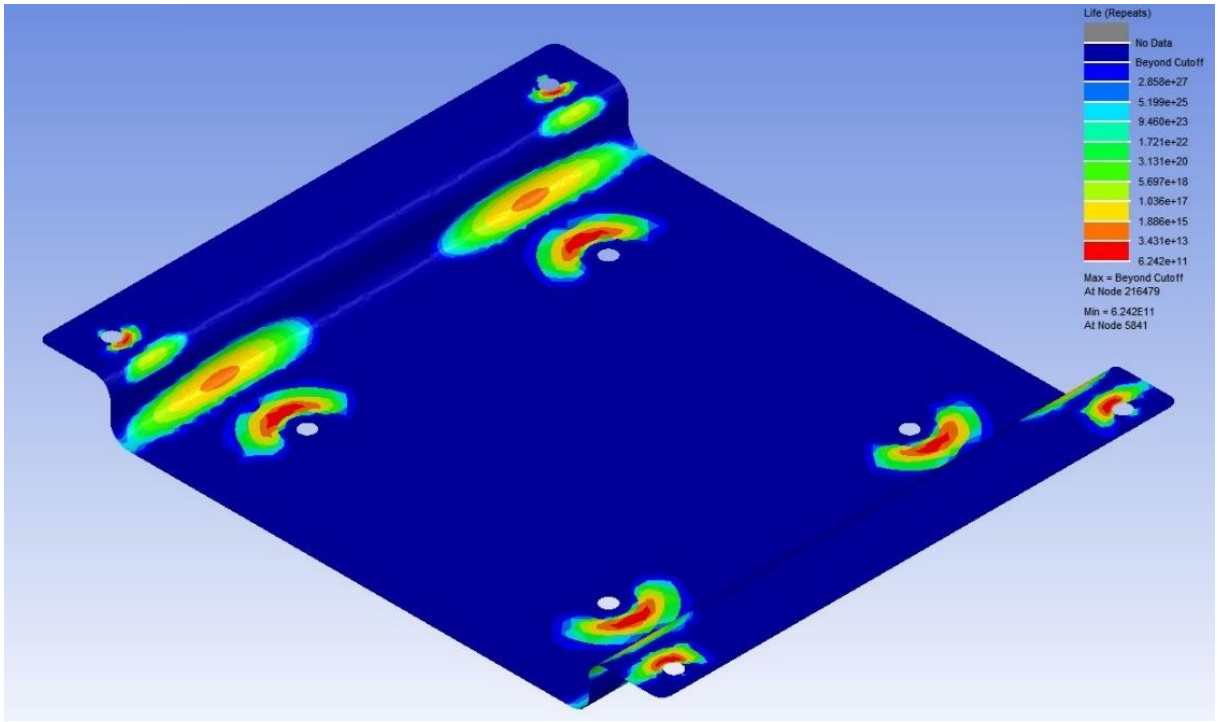

Figure 5.14 Lalanne Method Fatigue Life Result

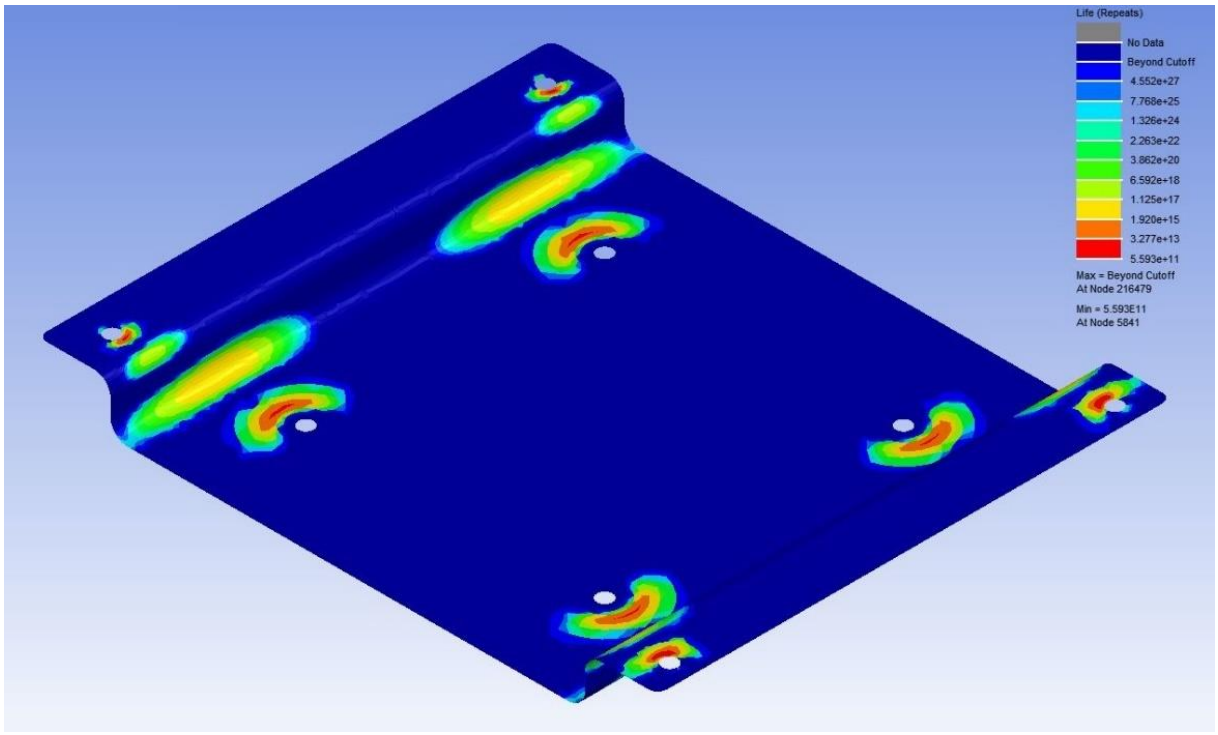

Figure 5.15 Dirlik Method Fatigue Life Result

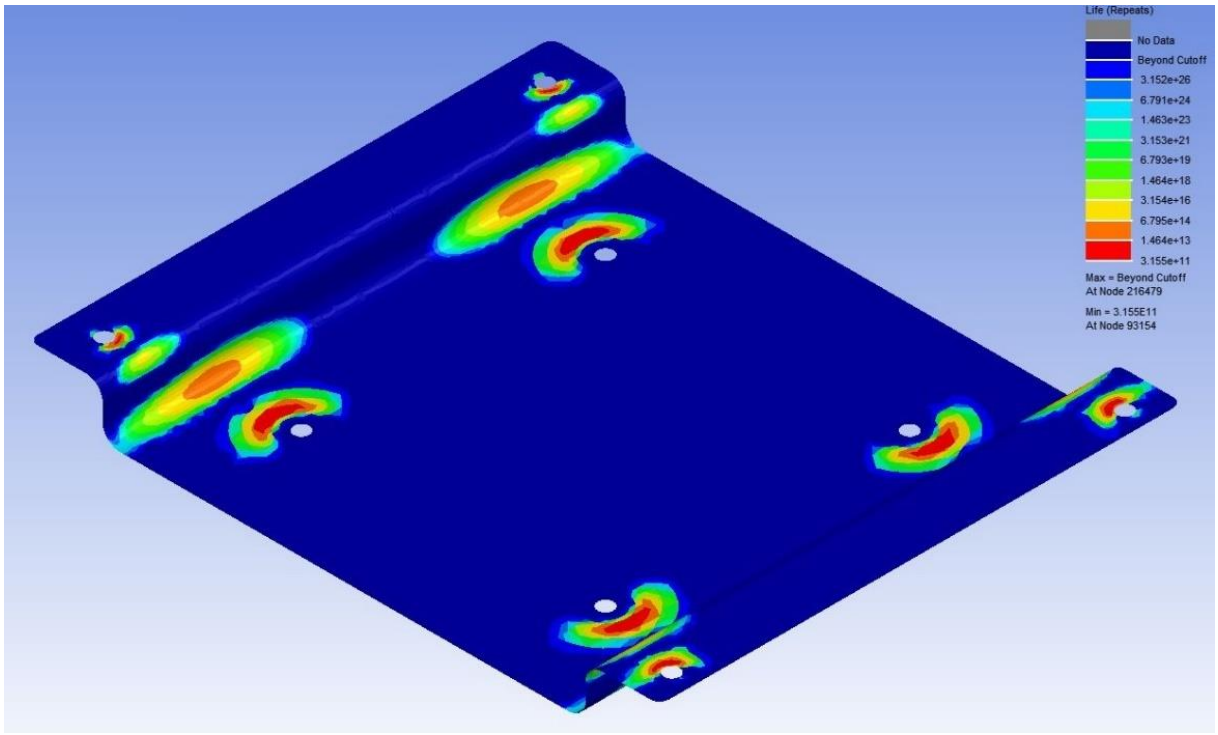

Figure 5.16 Narrow Band Method Fatigue Life Result

The stress PSD graph obtained by using the FRF and input power spectral density is given in Figure 5.17. The graph shows that the amplitudes of the stresses in the structure are quite low.

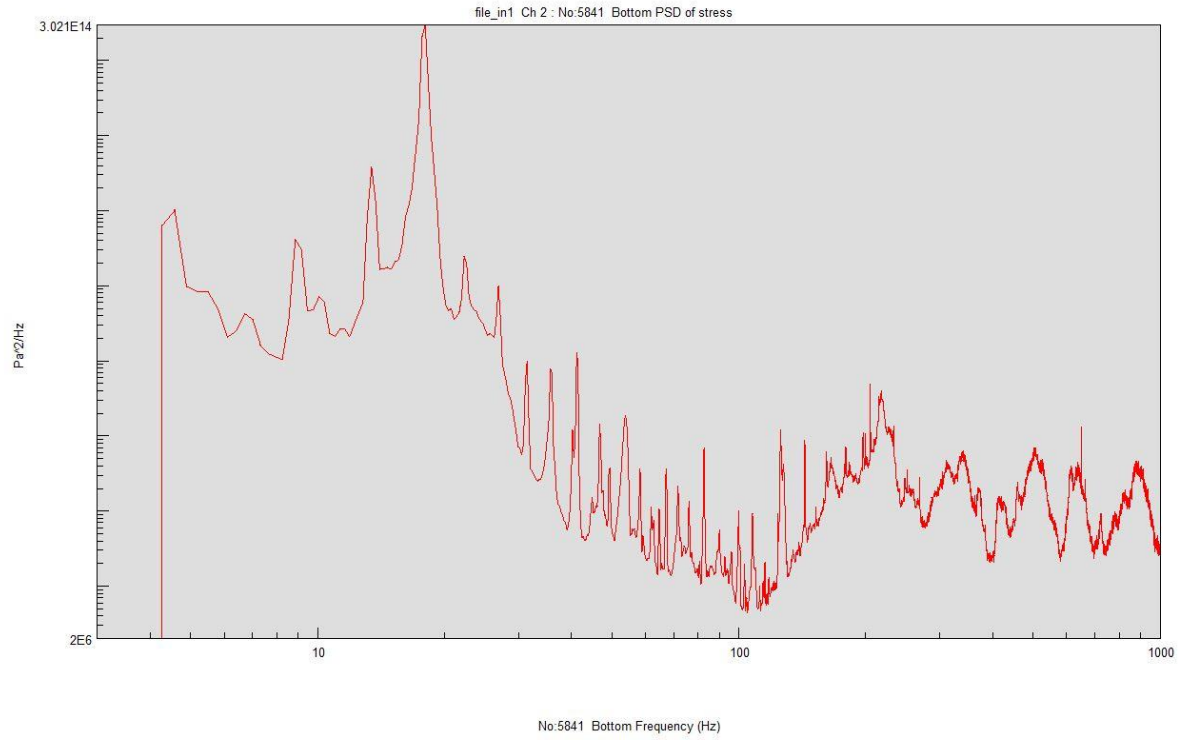

Figure 5.17 Stress PSD for 2500 Hours Input PSD

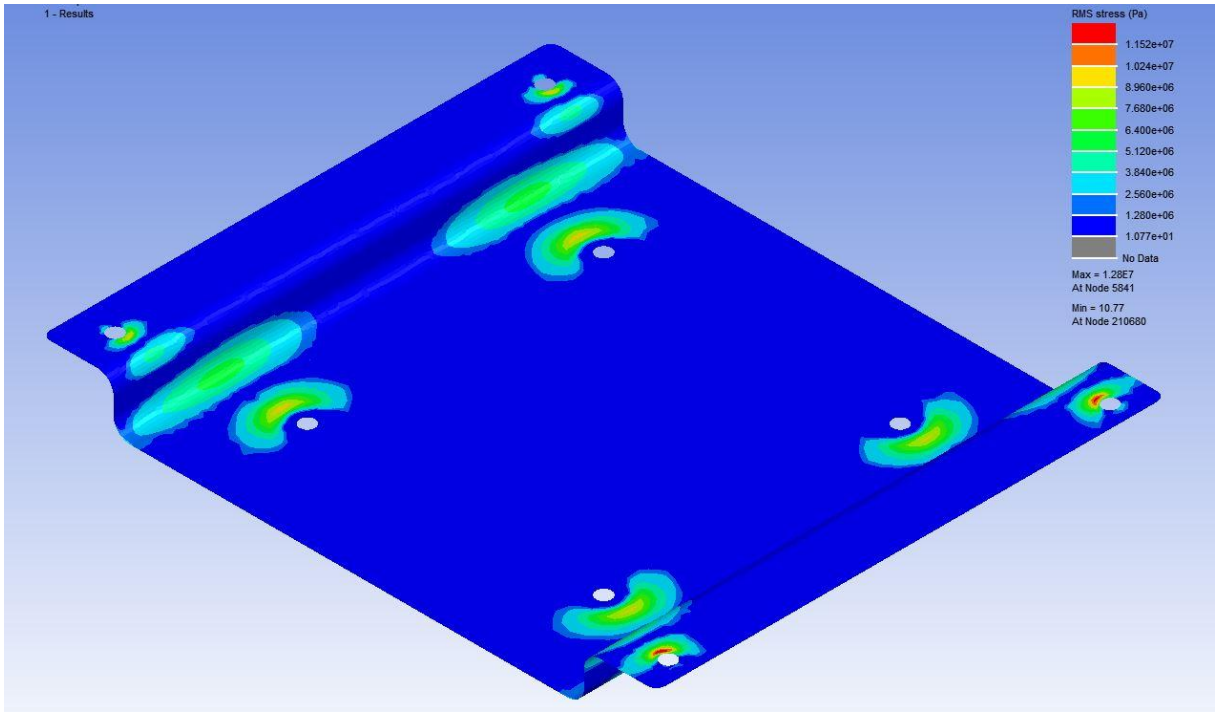

Figure 5.18 RMS Stesses for 2500 Hours Input PSD

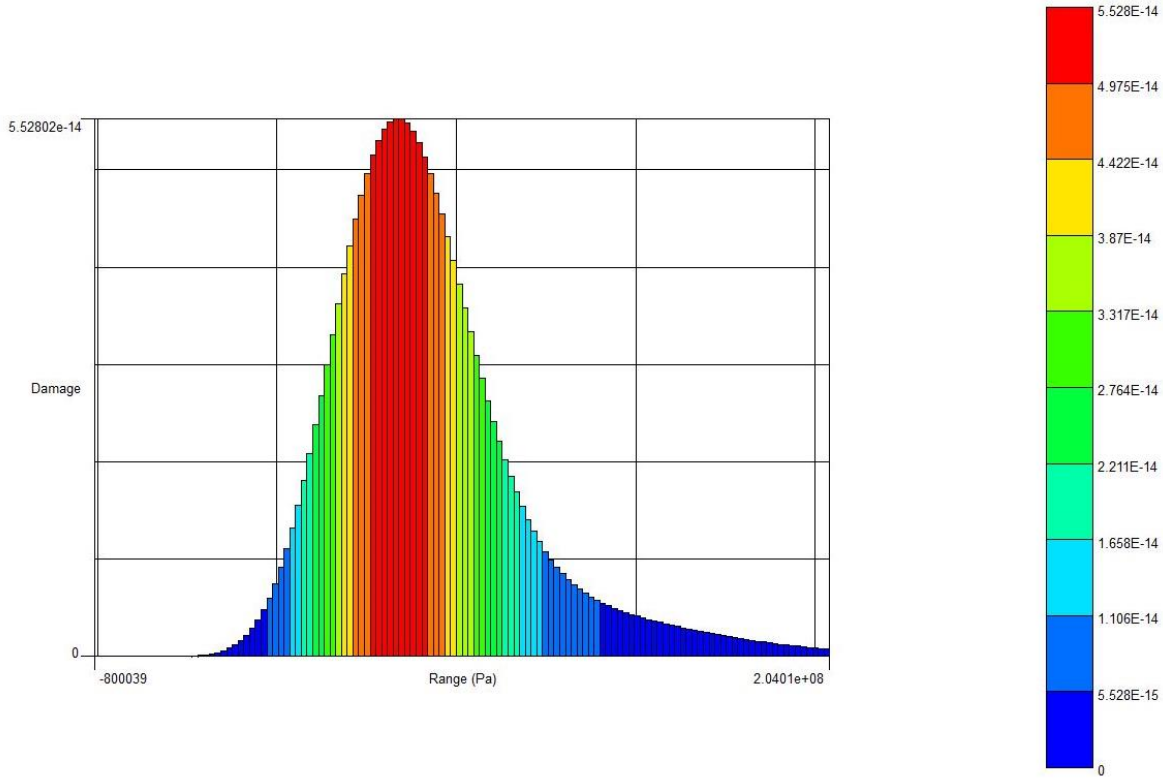

Figure 5.19 Dirlik Method Damage Histogram

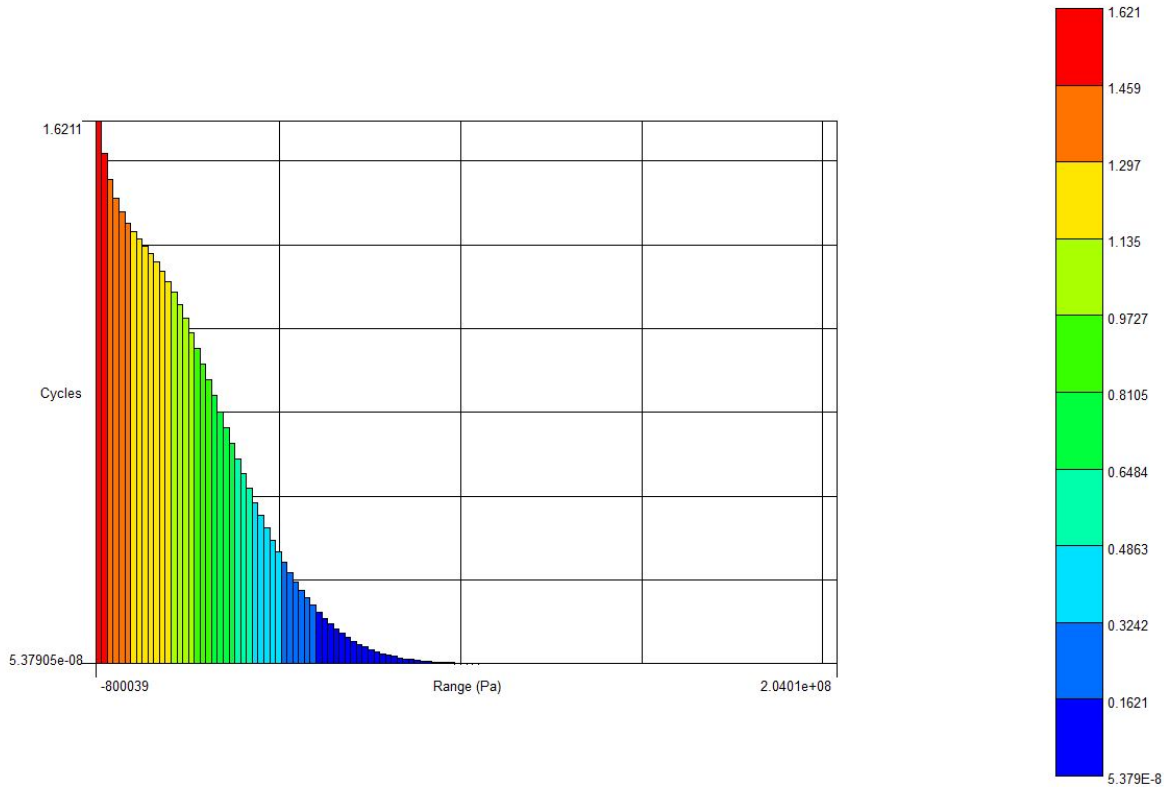

Figure 5.20 Dirlik Method Damage Histogram

5.5. Accelerated Life Test

In order to determine the accuracy of the analysis results, they must be compared with the test results. For this purpose, 2500 hours' data is accelerated to 4 hours, as it is suggested in the military standard. The PSD profile is obtained as given in Figure 4.3. Fatigue life analyzes were repeated for this profile and the results are given below.

Table 5-4 Fatigue Life Analysis Results for 4 Hours PSD

Cycle Counting Method	RMS Stress [Mpa]	Damage	Life [s]	Life [h]
Lalanne	30.2	5.545e-9	1.804e+08	5.011e+04
Dirlik		5.973e-9	1.674e+08	4.650e+04
Narrow Band		1.476e-8	6.773e+07	1.881e+04

The fatigue life of the part still has not reached the pratical test duration, i.e. the time required for damage to be observed is still very high.

A new PSD was created to excite the natural frequencies of the mount, as amplifying the flight data enough to be used in tests would exceed the shaker's limits, and the amplification at low frequencies could damage the absorber. The analysis was repeated using this PSD.

Table 5-5 Fatigue Life Analysis Results for Test PSD

Cycle Counting Method	RMS Stress [Mpa]	Damage	Life [s]	Life [min]
Lalanne	68.5	1.046e-4	9561	159.4
Dirlik		7.516e-5	13300	221.6
Narrow Band		2.548e-4	3925	65.4

As a result of the test, which is performed to observe the fatigue life and compare with the analysis results, the part was damaged after 191 minutes. Both Lalanne and Dirlik method gives the same difference from the test results. The Narrow Band method, on the other hand, gave the farthest result. The reason for this is that the irregularity factor of 0.398 is far from 1. The irregularity factor obtains information on whether the signal is a narrowband or a wideband signal. Since the irregularity factor is not close to 1, the signal doesn't have narrowband characteristic.

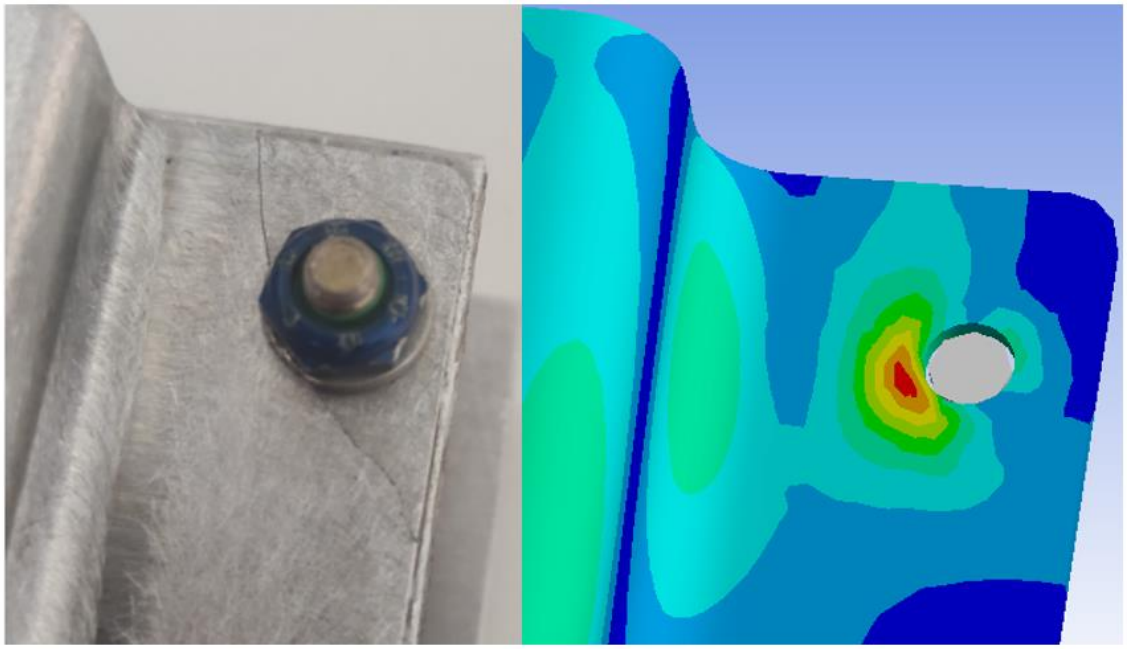

Figure 5.21 Fracture on the Mount and Finite Element Model

5.6. Case Study I

To see the effect of the absorbers on the life of the mount, the system is reconstruct without the absorber. The aluminum block is modeled as a point mass with the same weight and inertia. The contact surfaces were not changed and the damping coefficient was assumed to be 0.02 for all modes. Fatigue life analyzes were repeated for the 2500 hours profile and the results are given in Table 5-6.

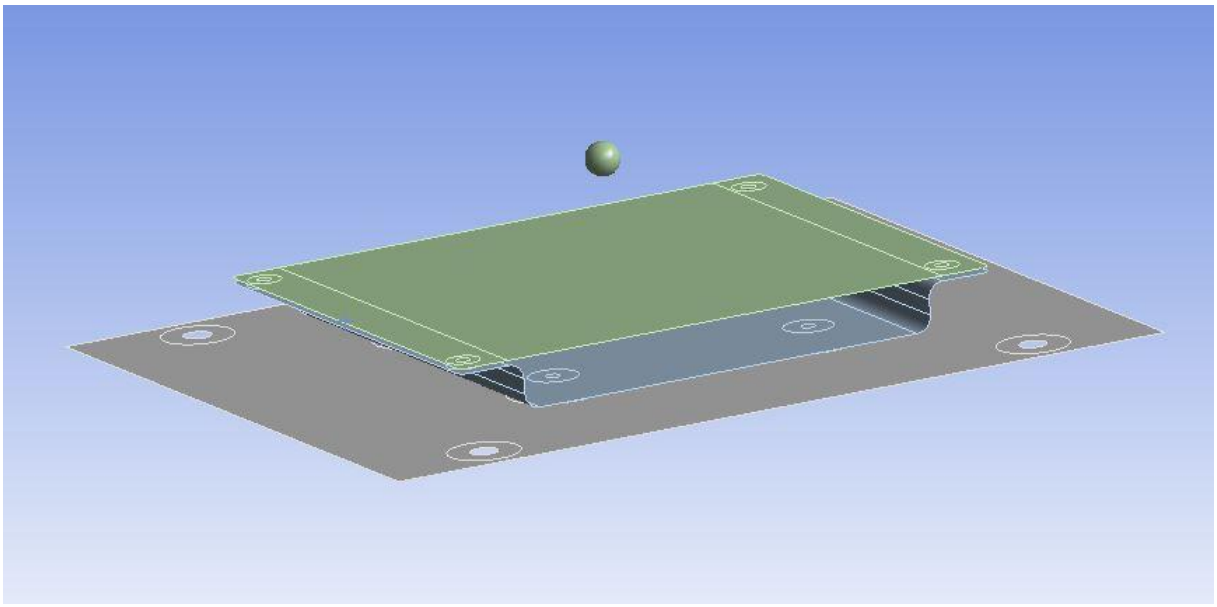

Figure 5.22 ANSYS Model of the System Without Absorbers

Table 5-6 Fatigue Life Analysis Results for the Mount Without Absorbers

Cycle Counting Method	RMS Stress [Mpa]	Damage	Life [s]
Lalanne	82.09	4.039e-4	2476
Dirlik		3.298e-4	3032
Narrow Band		4.826e-4	2072

When the system is reconstruct without the absorber, The natural frequencies of the new system are different from the original one. Since this modification affects the FRF data, the results of the fatigue life analysis, which is performed with the same input PSD, change.

5.7. Case Study II

2500 hours of PSD data are accelerated to 4 hours with using Equation (15). The value of m which is the scaling factor, used as 7.5, which is the recommended value in the standard for random environments. However, this m value is not provide same damage value with original PSD. To fix this undesirable situation, the value m is increased until the same damage is achieved.

Table 5-7 Fatigue Life Analysis Results for Diffrent m Values

m	Duration [h]	gRMS	Damage	RMS Stress [MPa]
-	2500	0.66	1.442e-5	12.8
7.5	4	1.55	7.985e-5	30.2
9.5	4	1.30	1.442e-5	25.2

Table 5-7 shows that m=7.5 value in the military standard will give more conservative results. The value of "m" is strongly influenced by the material S-N curve and this curve is not a linear plot. When the stresses used by Miner's theorem change, the area used in the S/N curve and the slope of the curve are also changes. Therefore, the value of m depends on the stress level of the structure and the S/N curve of the material.

6. CONCLUSION AND DISCUSSION

In this thesis, the fatigue life of a mount of a device with shock absorber is investigated with the real vibration data from flight conditions. All stages of the analysis have been verified by different tests. Fatigue life is calculated using three different methods because it is not known which method will give more accurate results without testing.

Vibration data that were measured from the aircraft were taken only once. The reason for this is that all measurements to be made have the same mean value because the vibration characteristic is ergodic random. This shows that the PSD graph to be created will not change even if the measurements are repeated.

In this thesis, the absorber is studied only as an element that changes the dynamic characteristics of the structure. The life of the absorber was not investigated. It has been assumed that the performance of the absorber does not change with factors such as temperature, abrasion, etc. throughout the tests and analyzes.

The use of the avionics unit itself in the tests was not preferred as it would cause the modes of the electronic board, components and other mechanical parts inside the device to appear in the results. Instead, an aluminum block of the same weight was used in the tests.

Since the material of the absorber has non-linear characteristics, it is not suitable to use in modal analysis. Instead, the absorber was modeled using spring connections on 3 axes. The spring connection uses the stiffness and damping coefficients. In order to obtain these values, a test setup containing only the absorber and the block was prepared. The necessary values were found from the results of the vibration test performed with this setup. The stiffness of the system was found using the natural frequency and mass of the system, and the damping coefficient was calculated with the Half-Power Method over the FRF data.

While preparing the finite element model of the whole system, a vibration test was performed using a shaker to accurately determine the diameters of the connection types and connection areas. To match the natural frequencies found as the result of the test, a parametric study was carried out with the connections. The study showed that the variation of connection types and connection areas greatly affects natural frequencies.

With the FRF data obtained from the test, damping ratios were obtained for all modes. These damping ratios were entered into the analysis separately for each natural frequency.

For the damping value written in the spring connection to be used in the MSUP harmonic analysis, the reduced damped solver must be used.

Damping ratios significantly affect the stresses occurring at natural frequencies. Small changes in stresses also affect the life of the parts considerably due to the nature of the S/N curve. However, one of the difficulties in determining the damping ratios is that the damping ratio changes according to the level of the excitation.

ANSYS Random Vibration Analysis module is not suitable for fatigue analysis. The reason is that the element damping used in the spring connection can not work with Random Vibration. That's why nCode is used which gets the FRF data from MSUP Harmonic Analysis.

Fatigue analyzes were first performed with the vibration data measured from the aircraft. Since it was not possible to test with the results obtained, 2500 hours of data were accelerated to 4 hours with the equations given in MIL-STD-810 to see the damage in the parts during the test period. However, the time required for damage to be observed is still very high.

A new PSD was created to excite the natural frequencies of the mount, as amplifying the flight data enough to be used in tests would exceed the shaker's limits, and the amplification at low frequencies could damage the absorber. The analysis was repeated using this PSD and verified by testing. As a result of the test performed to observe the fatigue life and compare with the analysis results, the part was damaged after 191 minutes. Both Lalanne and Dirlik method gives the same difference from the test results. The Narrow Band method, on the other hand, gave the farthest result. The reason for this is that the irregularity factor of 0.398 is far from 1.

When 2500 hours of data are accelerated to 4 hours, the value of m which is the scaling factor, used as 7.5, which is the recommended value in the standard for random environments. However, this m value is not provide same damage value with original PSD. To fix this undesirable situation, the value m is increased until the same damage is achieved.

All parts contain a certain amount of imperfections and since the mount is a sheet metal produced by bending, there are cambers on the part and this situation creates uncertainty in the analysis. In addition, the change in the damping characteristic of the system according to the input increases the uncertainty. Considering all these, the results obtained within the scope of this study are satisfactory.

REFERENCES

[1] W.A.J. Albert, Uber Treibseile am Harz. Archiv fur Mineralogie, Georgnosie, Bergbau und Huttenkunde, 10, 1837, 215.

[2] Wikipedia, Fatigue (material), https://en.wikipedia.org/wiki/Fatigue_(material), Last accesed on, 03/04/2022.

[3] W.J.M. Rankine, On the causes of the unexpected breakage of the journals of railway axles, and on the means of preventing such accidents by observing the law of continuity in their construction., 1842, pp. 105-108.

[4] W. Schütz, A history of fatigue, Engineering fracture mechanics, 54, 1996, 263-300.

[5] J. Goodman, Mechanics Applied To Engineering, Longmans, Green and Co. John, London, 1899.

[6] J.A. Ewing, J. Humfrey, The Fracture of Metals under Repeated Alternations of Stress, Proceedings of the Royal Society of London Series I, 71, 1902, 79.

[7] O. Basquin, The exponential law of endurance tests, Proc Am Soc Test Mater, 1910, pp. 625-630.

[8] H. Gough, The Fatigue of Metals, Scott, Greenwood and Son, London, 1924.

[9] A. Palmgren, Die lebensdauer von kugellargern, Zeitshrift des Vereines Duetsher Ingenieure, 68, 1924, 339.

[10] M. Miner, Cumulative fatigue damage, Journal of applied mechanics, 12, 1945, A159-A164.

[11] L.F. Coffin Jr, A study of the effects of cyclic thermal stresses on a ductile metal, Transactions of the American Society of Mechanical Engineers, New York, 76, 1954, 931-950.

[12] L. Coffin, The problem of thermal stress fatigue in austenitic steels at elevated temperatures, Symposium on Effect of Cyclic Heating and Stressing on Metals at Elevated Temperatures, ASTM International, 1954.

[13] P. Paris, The growth of cracks due to variations in load: Ph. D. Thesis. Lehigh University, 1962.

[14] M. Matsuishi, T.J.J.S.o.M.E. Endo, Fukuoka, Japan, Fatigue of metals subjected to varying stress, 68, 1968, 37-40.

[15] W. Elber, The significance of fatigue crack closure, Damage tolerance in aircraft structures, ASTM International, 1971.

[16] S.O. Rice, Mathematical analysis of random noise. Selected papers on noise and stochastic processes, Dover, New York, 1954, 133-294.

[17] J.S. Bendat, Probability functions for random responses: prediction of peaks, fatigue damage, and catastrophic failures, 1964.

[18] J. Tunna, Fatigue life prediction for Gaussian random loads at the design stage, Fatigue & Fracture of Engineering Materials & Structures, 9, 1986, 169-184.

[19] P.H. Wirsching, M.C. Light, Fatigue under wide band random stresses, Journal of the Structural Division, 106, 1980, 1593-1607.

[20] G. Chaudhury, W. Dover, Fatigue analysis of offshore platforms subject to sea wave loadings, International Journal of Fatigue, 7, 1985, 13-19.

[21] D.S. Steinberg, Vibration analysis for electronic equipment, 2000.

[22] T. Dirlik, Application of computers in fatigue analysis, 1985.

[23] N.W. Bishop, F. Sherratt, Finite element based fatigue calculations, NAFEMS, 2000.

[24] M. Aykan, Vibration fatigue analysis of equipments used in aerospace, 2005.

[25] Y. Eldoğan, Vibration fatigue analysis of structures installed on air platforms, 2012.

[26] S. Kelly, Fundamentals of Mechanical Vibrations, 2nd Edition, McGraw-Hill, 2000.

[27] C. Silva, Vibration: Fundamentals and Practice, CRC Press, 2000.

[28] S. Rao, Mechanical Vibrations, 2nd Edition, Addison-Wesley Publishing, 2000

[29] J. Zhang, "The Application of Maxwell Elements for Modeling, Identification and Analysis of Passive and Semi-Active Vibration Systems," Department of Mechanical Engineering, University of Louisville, Kentucky, 2006.

[30] J. Zhang and C. M. Richards, "Parameter identification of analytical and experimental rubberisolators represented by Maxwell models," Elsevier Ltd, 2007.

[31] S. Kaul, Modeling Techniques for Vibration Isolation in Motorcycles, Milwaukee: University of Wisconsin, 2006.

[32] D. Cinarel, "Vibration Isolation of Inertial Measurement Unit," Mechanical Engineering Department, METU, Ankara, 2012.

[33] J.E. Shigley, Shigley's mechanical engineering design, Tata McGraw-Hill Education, 2011.

[34] Hawkyard, M., Powell, B.E., Stephenson, J.M., McElhone, M., “Fatigue Crack Growth from Simulated Flight Cycles Involving Superimposed Vibrations”, International Journal of Fatigue, 1999, Vol.21, pp.S59-S68.

[35] C. Lalanne, Mechanical vibration and shock analysis, fatigue damage, John Wiley & Sons, 2010.

[36] T.J.C. Irvine, Rainflow cycle counting in fatigue analysis, 2011

[37] A. Halfpenny, A frequency domain approach for fatigue life estimation, China Mechanical Engineering (中国机械工程), 1998, 11.

[38] MSC Software, Multiaxial Fatigue Theory, http://web.mscsoftware.com/training_videos/patran/Reverb_help/index.html#page/Fatigue%2520Users%2520Guide/fat_mulitaxial.07.5.html, Last accesed on, 12/04/2022.

[39] Ncode, 10 Common Mistakes in Fatigue Analysis, https://www.ncode.com/videos/10-common-mistakes-in-fatigue-analysis-2020, Last accesed on,12/04/2022.

[40] Kocer B., "VIBRATION FATIGUE ANALYSIS OF STRUCTURESUNDER BROADBAND EXCITATION," M.Sc. Thesis, Middle East Technical University, Ankara, 2010.

[41] MSC Fatigue Version 2003 User's Manual, MSC Software Inc., USA, 2003

[42] S. Özsoy, "Vibration induced stress and accelerated life analyses of an aerospace structure," M.S. - Master of Science, Middle East Technical University, 2006.

[43] M.K.J.U.D.o.D.W. Thompson, DC, USA, MIL-STD-810G environmental engineering considerations and laboratory tests, 2008

[44] P. Avitabile, Modal testing: a practitioner's guide, John Wiley & Sons, 2017.

[45] M. HDBK, 5J Metallic Materials and Elements for Aerospace Vehicle Structures, Department of Defense Handbook, 31, 2003.

APPENDICES

APPENDIX A

Damping Ratio Estimation

The half-power bandwidth method can be used to estimate the damping ratio and corresponding Q value from the frequency response function of a structure which has been excited by base motion or an applied force. Half power points can be found by multiplying the peak amplitude with 0.707, which is approximately equal to the -3 dB decrease of the peak amplitude in the logarithmic scale.

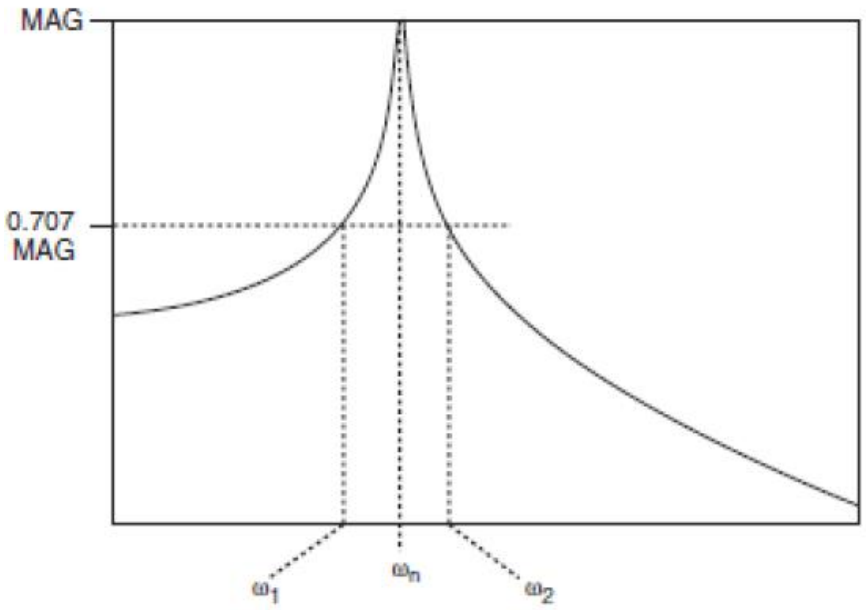

Figure A-1 Half-Power Bandwidth Method [44]

The damping ratio of each natural frequency location can be obtained with Equation (A.1).

$$\zeta = \frac{\omega_2 - \omega_1}{2.\omega_n} \tag{A.1}$$

APPENDIX B

Material Properties of Aluminum 2024 T3 and 6061-T6

Table B-1 Material Properties of Aluminum 2024 T3

Density	2.78 g/cc
Elastic Modulus	73.1 Gpa
Poisson Ratio	0.33
Fatigue Strength	138 Mpa
Ultimate Tensile Strength	483 Mpa
Yield Strength	345 Mpa

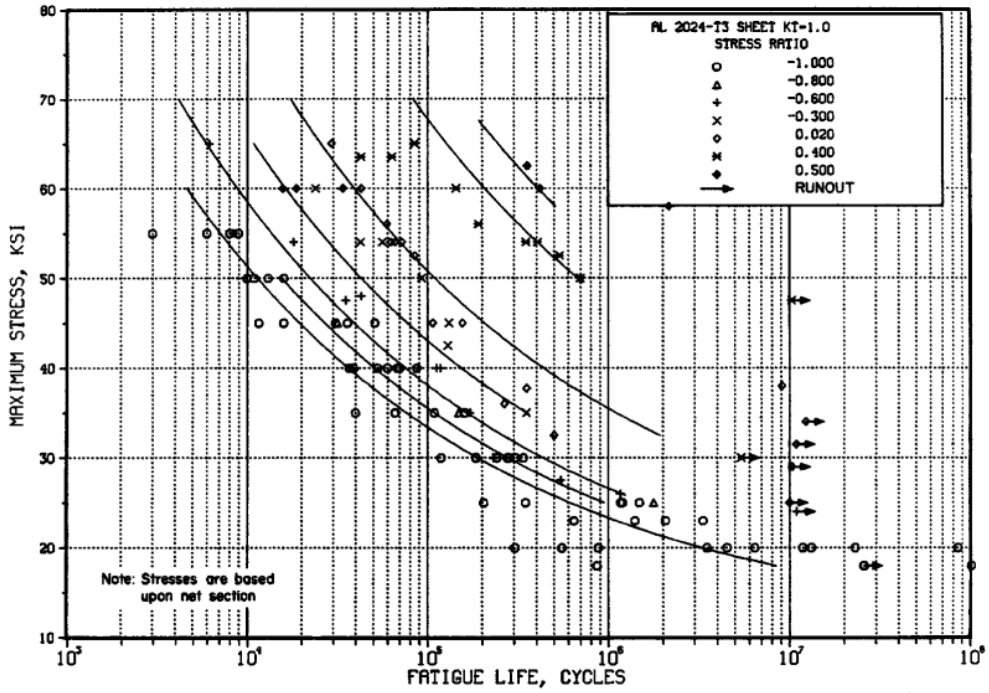

Figure B-1 Best fit S/N curve for unnotched 2024-T3 aluminum alloy [45]

Table B-2 Material Properties of Aluminum 6061-T6

Density	2.70 g/cc
Elastic Modulus	68.9 Gpa
Poisson Ratio	0.33
Fatigue Strength	96.5 Mpa
Ultimate Tensile Strength	310 Mpa
Yield Strength	276 Mpa

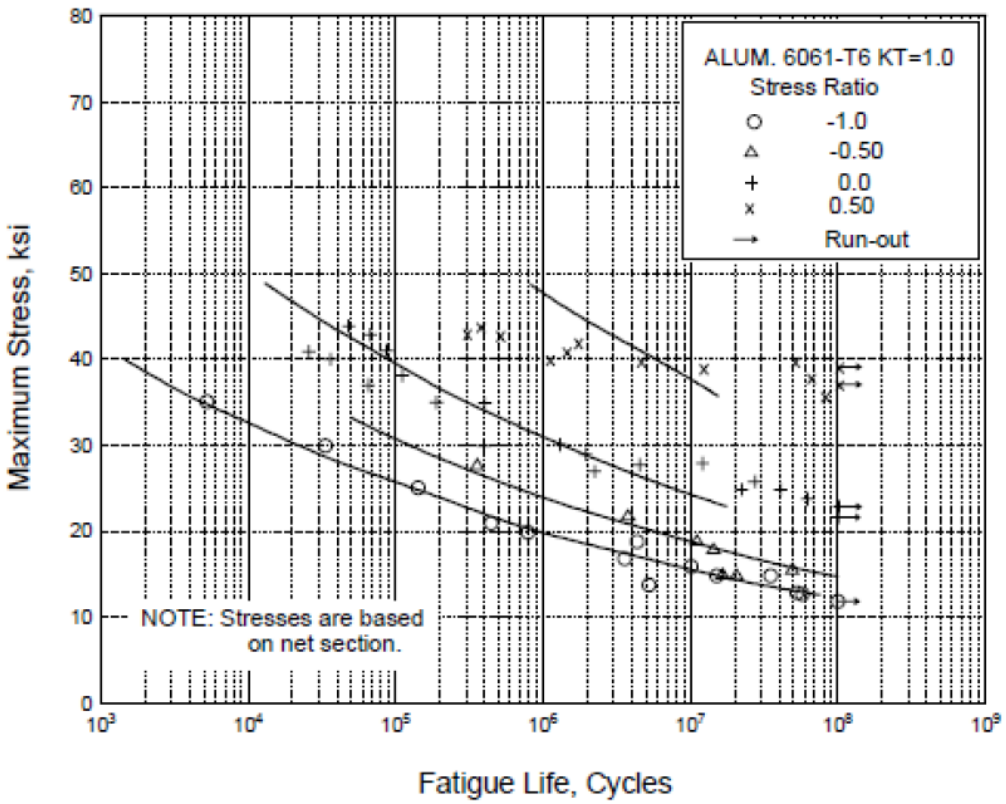

Figure B-2 Best fit S/N curve for unnotched 6061-T6 aluminum alloy [45]